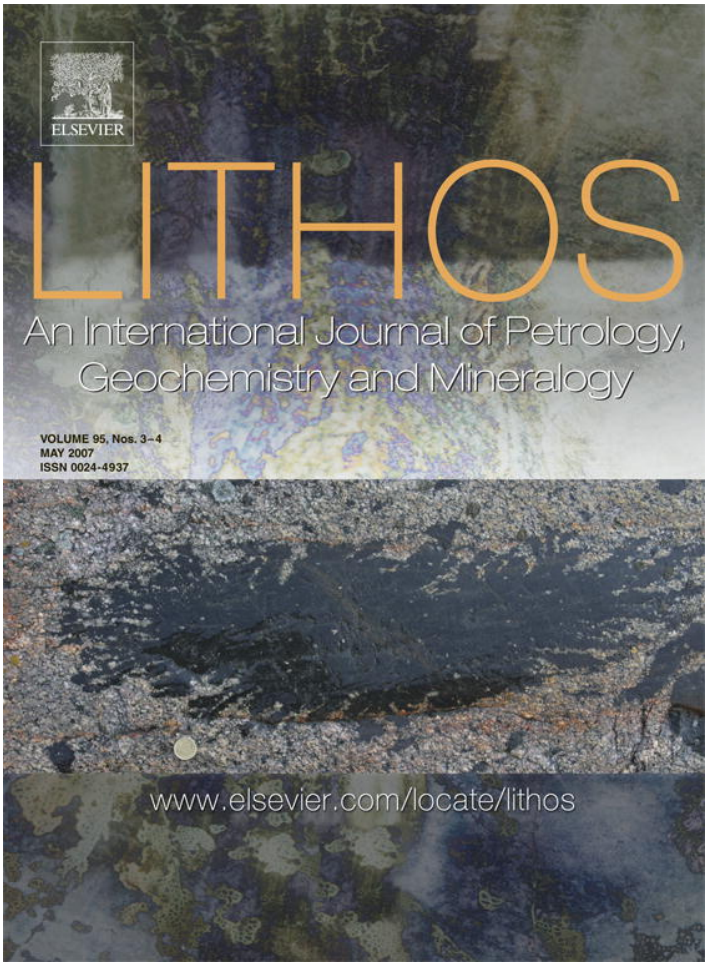

Available online at www.sciencedirect.com
ScienceDirect
Lithos 95 (2007) 208–228
LITHOS
www.elsevier.com/locate/lithos

Petrogenesis of A-type granites and origin of vertical zoning in the Katharina pluton, Gebel Mussa (Mt. Moses) area, Sinai, Egypt

Y. Katzir [a], M. Eyal [a], B.A. Litvinovsky [a,b,*], B.M. Jahn [c], A.N. Zanvilevich [a], J.W. Valley [d], Y. Beeri [a], I. Pelly [a], E. Shimshilashvili [a]

[a] *Department of Geological and Environmental Sciences, Ben-Gurion University of Negev, P.O. Box 653, Beer-Sheva 84105, Israel*
[b] *Geological Institute, RAS, 6a, Sakhyanova Str, Ulan-Ude 670047, Russia*
[c] *Institute of Earth Sciences, Academia Sinica, P.O. Box 1-55, Nankang, Taipei,11529, Taiwan*
[d] *Department of Geology and Geophysics, University of Wisconsin, Madison WI53706, USA*

Received 5 September 2005; accepted 17 July 2006
Available online 28 August 2006

Abstract

The central pluton within the Neoproterozoic Katharina Ring Complex (area of Gebel Mussa, traditionally believed to be the biblical Mt. Sinai) shows a vertical compositional zoning: syenogranite makes up the bulk of the pluton and grades upwards to alkali-feldspar granites. The latters form two horizontal subzones, an albite–alkali feldspar (Ab–Afs) granite and an uppermost perthite granite. These two varieties are chemically indistinguishable. Syenogranite, as compared with alkali-feldspar granites, is richer in Ca, Sr, K, Ba and contains less SiO_2, Rb, Y, Nb and U; Eu/Eu* values are 0.22–0.33 for syenogranite and 0.08–0.02 for alkali-feldspar granites. The $\delta^{18}O$ (Qtz) is rather homogeneous throughout the pluton, 8.03–8.55‰. The $\delta^{18}O$ (Afs) values in the syenogranite are appreciably lower relative to those in the alkali–feldspar granites: 7.59–8.75‰ vs. 8.31–9.12‰. A Rb–Sr isochron ($n=9$) yields an age of 593±16 Ma for the Katharina Ring Complex (granite pluton and ring dikes).

The alkali–feldspar granites were generated mainly by fractional crystallization of syenogranite magma. The model for residual melt extraction and accumulation is based on the estimated extent of crystallization (~ 50 wt.%), which approximates the rigid percolation threshold for silicic melts. The fluid-rich residual melt could be separated efficiently by its upward flow through the rigid clusters of crystal phase. Crystallization of the evolved melt started with formation of hypersolvus granite immediately under the roof. Fluid influx from the inner part of the pluton to its apical zone persisted and caused increase of P_{H2O} in the magma below the perthite granite zone. Owing to the presence of F and Ca in the melt, P_{H2O} of only slightly more than 1 kbar allows crystallization of subsolvus Ab–Afs granite. Abundance of turbid alkali feldspars and their $^{18}O/^{16}O$ enrichment suggest that crystallization of alkali-feldspar granites was followed by subsolvus fluid–rock interaction; the $\delta^{18}O$ (Fsp) values point to magmatic origin of fluids.

The stable and radiogenic isotope data [$\delta^{18}O$ (Zrn)=5.82±0.06‰, $I_{Sr}=0.7022\pm0.0064$, ε_{Nd} (T) values are +3.6 and +3.9] indicate that the granite magma was generated from a 'juvenile' source, which is typical of the rocks making up most of the Arabian–Nubian shield.

Keywords: A-type granite; Alkali-feldspar granite; Vertical zoning; Fractional crystallization; Oxygen and Sr–Nd isotopes

* Corresponding author. Department of Geological and Environmental Sciences, Ben-Gurion University of Negev, P.O. Box 653, Beer-Sheva 84105, Israel. Tel.: +972 8 6477522; fax: +972 8 6472997.
E-mail addresses: ykatzir@bgu.ac.il (Y. Katzir), moey@bgu.ac.il (M. Eyal), borisl@bgu.ac.il (B.A. Litvinovsky).

0024-4937/$ - see front matter © 2006 Elsevier B.V. All rights reserved.
doi:10.1016/j.lithos.2006.07.013

1. Introduction

The worldwide distribution of A-type granites has been recognized more than 20 years ago (Loiselle and Wones, 1979; White and Chappell, 1983). The composition of A-type granites is diverse; they comprise syenogranite, peralkaline and alkali-feldspar granite and syenite, rapakivi granite, monzogranite and F-rich topaz granite (e.g. Collins et al., 1982; Whalen et al., 1987; Eby, 1992; Whalen et al., 1996; Patiño Douce, 1997). Therefore, along with the problem of the origin of the A-type granites (e.g. Whalen et al., 1987; Eby, 1990; Whalen et al., 1996; Wu et al., 2002; Bonin, 2004, and many others), possible genetic links between the different varieties of the A-type granites are of particular interest. In the vast crustal provinces of Central Asia and the Arabian–Nubian Shield (Bentor, 1985; Wickham et al., 1995; Litvinovsky et al., 2002; Jahn, 2004) three rock types are dominant among the A-type granites: metaluminous syenogranite, alkali-feldspar (mostly perthitic) granite and peralkaline granite. Close consanguinity of alkali-feldspar and peralkaline granites is demonstrated in many localities (e.g. Zanvilevich et al., 1995; Whalen et al., 1996; Jahn et al., 2000; Litvinovsky et al., 2002; Jahn, 2004). However, the nature of links between silicic magmas, forming alkali-feldspar granite and oligoclase bearing syenogranite, has not been resolved.

The Katharina pluton is a central granite pluton of the Neoproterozoic Katharina Ring Complex located in the southern Sinai Peninsula, Egypt. It is made up of syenogranite and alkali-feldspar granite. The two rock types are confined to different levels of the pluton and thus define its vertical zoning. In this paper, we present chemical and isotope data to constrain the likely processes responsible for the zoning of the Katharina pluton and formation of alkali-feldspar granite.

2. Geological setting

The Katharina Ring Complex is a typical Late Pan-African granitoid ring complex in the Arabian–Nubian Shield. Along with numerous A-type granite plutons, it was formed in the last stage of the Shield evolution, when a fundamental transition in tectonic style, from compressional to extensional, occurred 620–600 My ago (Gass, 1982; Stern et al., 1984; Bentor, 1985; Kröner et al., 1987; Stern, 1994; Genna et al., 2002; Meert, 2003). The Katharina Complex is situated in the high mountainous area of the Sinai Peninsula (Fig. 1). Gebel Mussa, the mountain in the central part of the Complex, is traditionally believed to be the biblical Mount Sinai. The total area of the Complex is over 400 km^2. Country rocks include a volcaniclastic suite (Rutig volcanics), a calc-alkaline plutonic series represented by diorite and various granites, and a granitic gneiss.

The formation of the Katharina Ring Complex occurred in three stages. It commenced with the extrusion of the Katharina volcanics including peralkaline ignimbrite and trachyrhyolite. Along with flows, tuffs and volcanic breccia, a number of subvolcanic bodies of peralkaline granophyre and quartz syenite porphyry were emplaced (Goor, 1982). Two ring dikes mark the second stage of the Complex formation. The larger Outer Ring Dike is about 30 km in diameter and up to 1.5 km wide. It is steeply dipping at an angle of 70–80° inward and is intruded by the Katharina pluton. The dike is built by emplacement of quartz monzonite porphyry, quartz syenite porphyry and alkali-feldspar granophyre (Fig. 1). The Inner Ring Dike is similar in composition. At present only the eastern half of the Inner Ring Dike is preserved to the south of Gebel Mussa (Fig. 1); the western half was eliminated by the intrusion of the Katharina pluton.

The emplacement of the *Katharina pluton* occurred in the third stage of development of the Complex. The pluton is roughly oval-shaped, with NE–SW orientation, and occupies an area of 210 km^2. Several small stocks that are likely projections of a larger unexposed body accompany the pluton. The pluton has a fairly flat upper surface and steeply dipping walls (Fig. 2, cross section). In the southwestern part (area of Gebel Bab) a projection of 4 by 3 km in area and 300 m high is inferred. At the northern end, the pluton intrudes the country rocks as a dike more than 1 km wide that narrows gradually over a distance of 20 km into a horse-tail splay of small dikes about 5 m wide. The contact of granites with country rocks is sharp, without evidence of metasomatic alteration. In the 40–60 m thick marginal zone below the flat roof the grain size of the granite slightly decreases and irregular patches of porphyritic varieties appear. Porphyritic varieties are characteristic of all types of granites making up the pluton. Plutonic rocks are cut by pegmatite veins of a few decimeters to few dozen meters, and narrow aplite and microgranite dikes. Not infrequently pegmatites form lenses and pockets in granite. During the Neogene the pluton was tilted about 5° to the north and its eastern part was uplifted by ~ 1 km along a major fault (Eyal and Hezkiyahu, 1980).

The granite was emplaced at shallow depth, as evidenced by fine-grained and porphyritic marginal zones, as well as by the thickness of the volcanic roof that is slightly more than 1–1.5 km (Eyal and Hezkiyahu, 1980). Judging from the size of the volcanic caldera

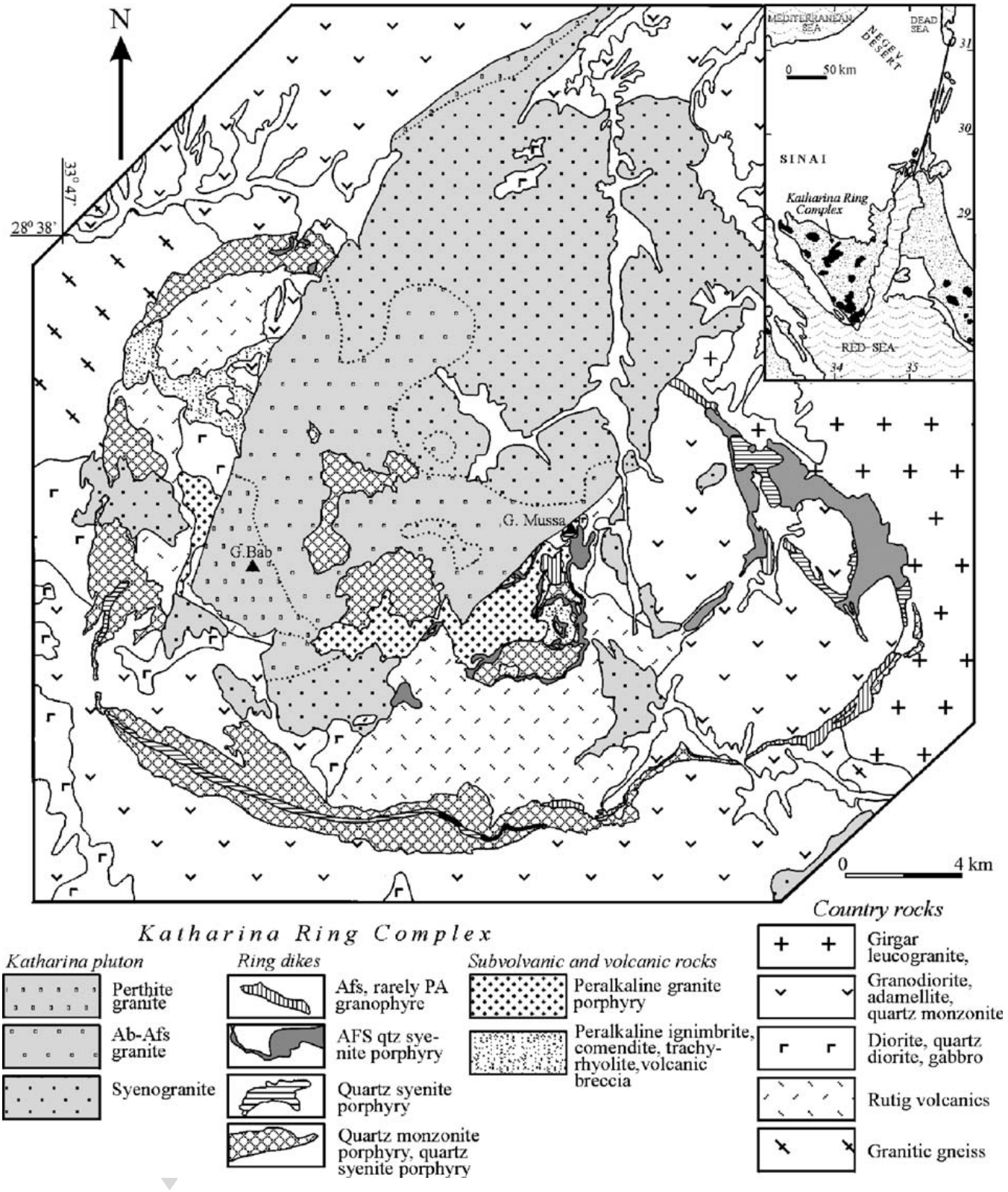

Fig. 1. Schematic geological map of the Katharina Ring Complex. *Inset*: Location of the Katharina Ring Complex and related alkaline granite plutons in Sinai Peninsula and adjacent areas.

intruded by the Katharina pluton (30 km in diameter), the thickness of the volcanic section at the time of emplacement was hardly more than 2–3 km.

Vertical compositional zoning in the pluton is established by detailed sampling and petrographic study of large polished slabs. The full body of results obtained

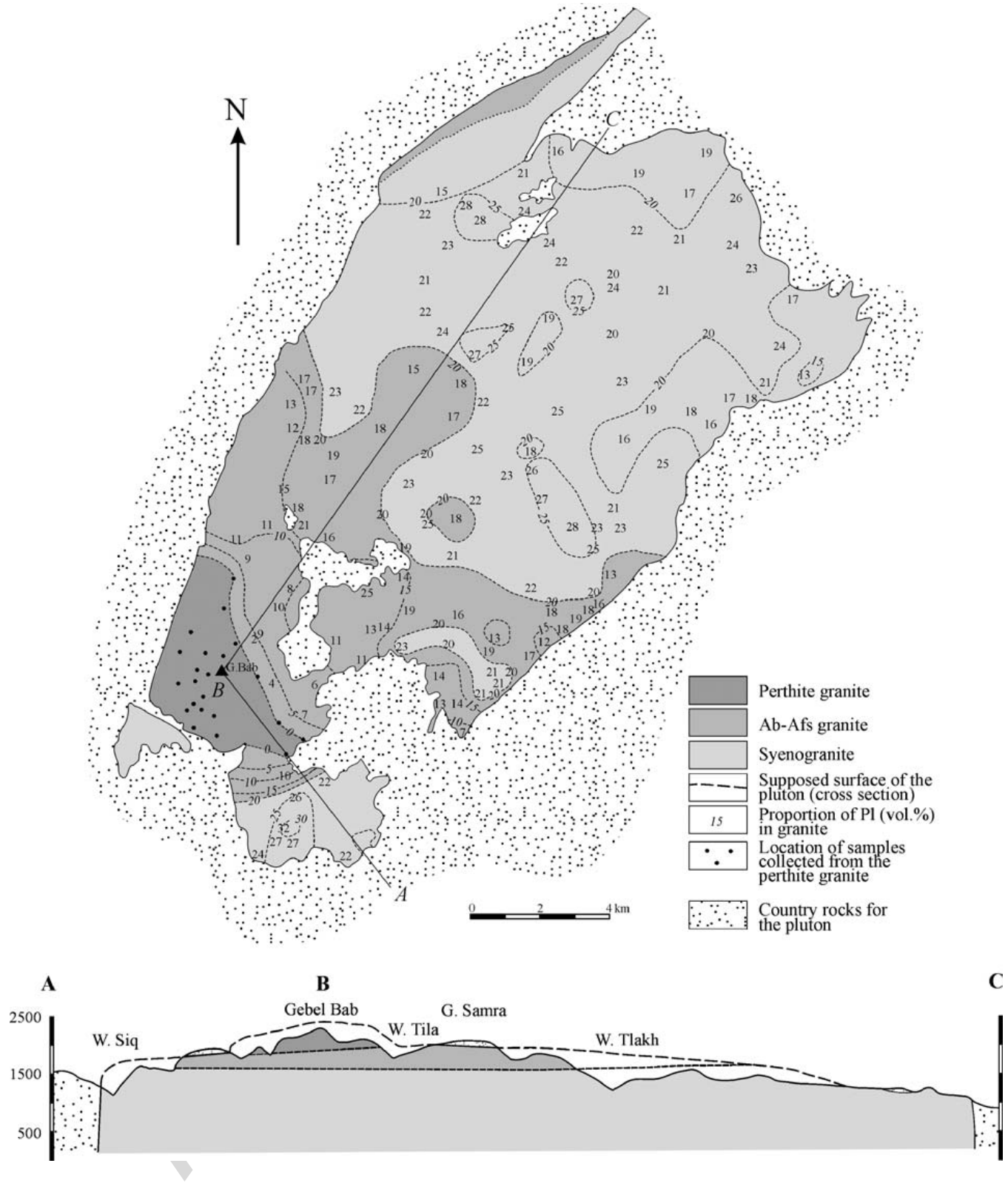

Fig. 2. Distribution of plagioclase (vol.%) in the Katharina granites, and schematic cross section along the pluton.

was published by Eyal and Hezkiyahu (1980); here only the most illustrative map of plagioclase distribution (Fig. 2) and data on representative modal compositions (Table 1) are given. The results show that the bulk of the pluton volume is made up mainly of syenogranite (Fig. 2). The highest elevations (the Gebel Bab area in its SW part) consist of perthite granite. The maximum thickness of the perthite granite zone is more than 500 m.

The 300–500 m thick zone below the perthite granite is made up of albite–alkali feldspar (Ab–Afs) granite. The boundary surfaces of the three zones are nearly horizontal (see cross-section in Fig. 2). The transition from syenogranite to Ab–Afs granite is poorly discernible in outcrops and only recognized by the decrease in plagioclase content (approximately ≤20 vol.%, Table 1) and change of its composition to albite. Going upwards in the pluton, the proportion of plagioclase in Ab–Afs granite decreases systematically to 2–4% (Fig. 2). The contact between the Ab–Afs and perthite granite is also gradational, and it becomes more distinguishable due to the color contrast with the redder perthite granite.

Table 1
Modal composition of representative granites from the Katharina pluton, vol.%

Sample no.	Perthite	Plagioclase	Quartz	Mafic, opaque
Syenogranite				
D163	46.1	25.3	26.3	2.3
D165	40.7	25.5	29.8	4
D82	40.2	2.2	36.1	2.6
D85	42.1	23.4	29.9	4.6
D135	40.2	27.6	31.4	0.8
D26	39	27.8	30.3	2.9
D109	50.1	19.2	29.2	1.5
D111	51.5	21.6	24.9	2
D113	49	20.3	29	1.7
D148	49.6	20.4	28	2
D156	45.8	22.1	28.7	3.4
Albite–alkali feldspar (Ab–Afs) granite				
D97	40.7	19.6	37.1	2.6
D54	65.2	4	27.3	3.5
D59	56	10.9	31.4	1.7
D93	48	17.2	31	3.8
D100	45.5	20	31.8	2.7
D63	51.7	8.3	37.2	2.8
D67	53	10.7	34.6	1.7
D72	50	13.3	36	0.7
D99	46.5	16.1	35.9	1.5
D122	46.4	19	33.2	1.4
D123	51	14.4	31	3.6
Perthite granite				
D43	63.6	0.0	33.5	2.9
D40	65.6	0.0	32.2	2.2
D33	68.6	0.0	29.3	2.1
D37	62.6	0.0	34.5	2.9
D49	66.4	0.0	29.7	3.9
D51	66.8	0.0	30.5	2.7
D52	65.2	0.0	33.1	1.7
D69	64.3	0.0	34	1.7

The mol.% of An in plagioclase ranges mostly from 8 to 20 in syenogranite; in Ab–Afs granite it varies from 0 to 7.

3. Analytical methods

3.1. Petrography

In addition to common thin section study, a total of 189 specimens representing the entire exposed pluton, averaging one specimen/km^2 and covering an altitude from 900 m to more than 2200 m above sea level, were used for modal analysis. A polished surface of ~ 150 cm^2 was prepared for every sample; 1000 points covering at least 100 cm^2 were counted (see details in Eyal and Hezkiyahu, 1980). The minerals counted were plagioclase, perthite, quartz and mafic minerals including opaques. Special investigation was performed for detailed study of perthites. The volume proportion of *Ab* and *Or* phases in perthites was measured by counting 4000 points in regular thin sections using a magnification of ×100 or ×250. The quantitative method (see details in Eyal and Shimshilashvili, 1988) was applied for studying the distribution of various perthite textures in alkali feldspar and the total amount of Ab in perthites from different granite types.

3.2. Mineral chemistry

The mineral chemistry of biotite and feldspars was determined by a JEOL JXA-8600 electron microprobe at the Hebrew University of Jerusalem. Electron beam conditions were 15 keV and 10 nA. The results were corrected by the ZAF method. The detection limits are 0.05–0.09 wt.% for Na_2O, MgO, Al_2O_3, and SiO_2; 0.01–0.05 wt.% for Cl, K_2O, CaO, TiO_2, MnO, and FeO; and 0.3–0.4 wt.% for F.

3.3. Geochemistry

Major element contents were determined by ICP-AES at the Geological Survey of Israel (Jerusalem), and trace element including REE contents by ICP-MS at CRPG-CNRS, Nancy, France and at IGEM, Moscow, Russia. Some samples were analyzed by XRF and instrumental neutron activation at the Analytical Center of Geological Institute, Russian Academy of Sciences (Moscow). Analyses are considered accurate to within 2–5% for major elements, and better than 10–15% for trace elements. The accuracy for all the REE (except Lu) is 1–5%, for Lu 9–10%.

Oxygen isotope analyses were performed using the laser fluorination technique at the University of Wisconsin-Madison. BrF_5 was used as the reagent. Oxygen was purified cryogenically and with an inline Hg diffusion pump, converted to CO_2 using a hot

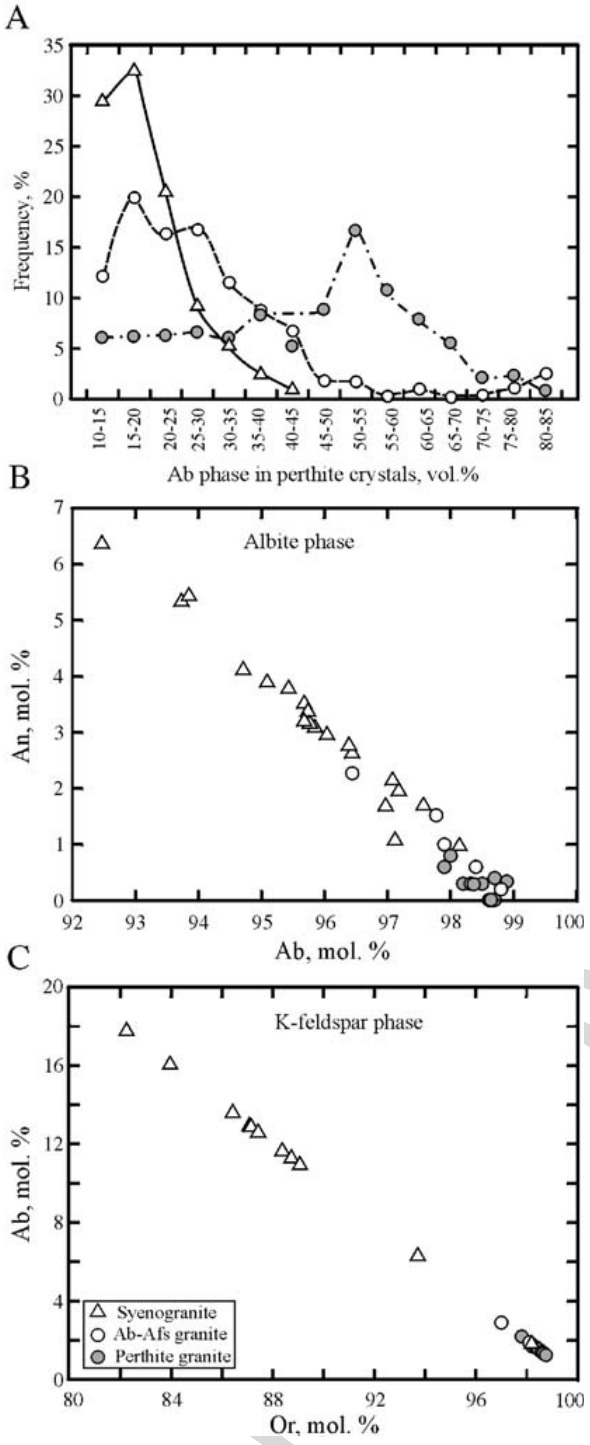

Fig. 3. Characteristics of perthites from the Katharina granites. A=proportion of exsolved Ab phase in perthite grains, B and C=correlation between *Ab–An* contents in albite (B) and *Or–Ab* contents in K-feldspar (C) phases of perthite.

graphite rod, and analyzed on a Finnigan MAT 251 mass spectrometer (Valley et al., 1995). Quartz separates (1.5 to 2 mg/analysis) were analyzed using the rapid heating, defocused beam technique (Spicuzza et al., 1998a). Plagioclase and K-feldspar separates, which might react appreciably with BrF_5 at room temperature, were analyzed (2 to 2.5 mg/analysis) using an 'air-lock' sample chamber (Spicuzza et al., 1998b). Two out of fifteen 'air lock' feldspar analyses were duplicated with average reproducibility of ±0.1‰. Quartz separate analyses were not duplicated; however, the long-term reproducibility for quartz analysis in the UW isotope lab is ±0.1‰. During each analytical day at least four aliquots of UW Gore Mountain Garnet standard (UWG-2) were analyzed. The overall average for 40 analyses of UWG-2 closest in time to the quartz analysis was 5.61± 0.09‰. The average value of UWG-2 during 'air lock' analysis was 5.48±0.10‰ (n=26). Quartz and feldspar data were adjusted by an average of 0.17 and 0.32‰, respectively, determined by the difference between each day's UWG-2 value and 5.8‰, the accepted $\delta^{18}O$ value of UWG-2 (Valley et al., 1995).

3.4. Rb–Sr and Sm–Nd isotopes

Isotope ratios were measured at the Universite de Rennes, France. The analytical techniques are detailed in Jahn et al. (1996). Mass analyses were performed using a 7-collector Finnigan MAT-262 mass spectrometer in static mode for Sr and dynamic mode for Nd. $^{87}Sr/^{86}Sr$ ratios were normalized against the value of $^{87}Sr/^{86}Sr=0.1194$. Long-term replicate analyses (>150) on NBS-987 Sr standard yielded $^{87}Sr/^{86}Sr=0.710259\pm5$ (2σ), but the three analyses obtained during the course of work gave an average of 0.710235 (see Table 6). The reported Sr isotopic ratios have been adjusted to NBS-987= 0.710250. $^{143}Nd/^{144}Nd$ ratio were normalized against the value of $^{146}Nd/^{144}Nd=0.7219$. Long-term replicate analyses (>150) on an in-house (Rennes) Ames Nd standard gave $^{143}Nd/^{144}Nd=0.511966\pm5$ (2σ), which is

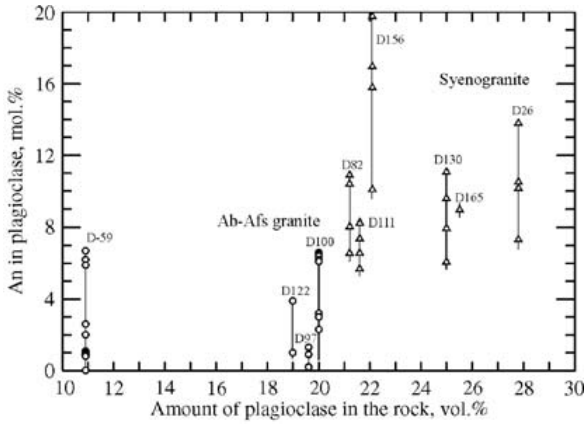

Fig. 4. Graph showing the correlation between the amount of plagioclase in the rocks (syenogranite and Ab–Afs granite) and *An* content in the plagioclase.

Table 2
Representative microprobe analyses of biotite from the Katharina pluton (wt.%)

Sample no.	D10	D156	D100	D82	D26	D97
	Syenogranite					Ab–Afs granite
n	1	2	4	2	3	2
SiO_2	36.08	36.89	37.61	37.58	38.94	38.23
TiO_2	2.21	2.78	2.63	3.23	2.18	1.32
Al_2O_3	16.67	12.10	16.49	12.16	13.67	19.84
FeO*	25.34	23.02	23.38	23.91	16.16	19.73
MnO	2.70	1.33	3.68	1.47	1.53	3.17
MgO	2.93	9.36	3.18	8.18	12.09	1.56
CaO	0.00	0.08	0.05	0.00	0.00	0.04
Na_2O	0.20	0.26	0.30	0.15	0.16	0.17
K_2O	9.38	9.27	9.22	9.33	9.35	9.11
F	3.10	n.d	n.d	1.59	3.51	2.59
Cl	–	0.06	–	0.06	0.03	–
Total	98.60	96.01	96.63	97.66	97.61	95.75
F, Cl=O	1.30	0.01		0.68	1.49	1.09
Total, calc	97.30	96.00	96.53	96.58	96.12	95.51
Atoms to 11 oxygens						
Si	2.856	2.902	2.915	2.931	2.970	2.980
Al iv	1.144	1.098	1.086	1.069	1.03	1.020
Al vi	0.411	0.024	0.421	0.048	0.199	0.802
Ti vi	0.131	0.165	0.153	0.189	0.125	0.078
Fe	1.678	1.515	1.515	1.560	1.031	1.286
Mn	0.181	0.089	0.242	0.097	0.099	0.209
Mg	0.346	1.097	0.367	0.951	1.371	0.182
Ca	0.000	0.007	0.004	0.000	0.000	0.003
Na	0.031	0.024	0.044	0.023	0.024	0.026
K	0.947	0.931	0.911	0.928	0.910	0.906

(1) FeO*=total Fe calculated as FeO.
(2) Here and in Table 3, n.d.=not determined; hyphen=below the detection limit.
(3) *n*=number of analyzed grains.

equivalent to the La Jolla Nd standard of 0.511860. Isochron ages were calculated using the regression program ISOPLOT-3 (Ludwig, 2003). Input errors are 2% for $^{87}Rb/^{86}Sr$ and 0.005% for $^{87}Sr/^{86}Sr$. Unless specified, the errors quoted in age represent±standard deviation (2δ).

4. Petrography

All three main rock types from the Katharina pluton are leucocratic, mostly coarse- and medium-grained, commonly even-grained or mildly porphyritic.

The *syenogranite* is a grayish pink rock with grain size of 5–10 mm and hypidiomorphic texture. The average contents of alkali feldspar, quartz and plagioclase are 46, 30 and 22 vol.%, respectively (Table 1). Plagioclase forms prismatic crystals, not infrequently zoned. Alkali feldspar crystals are anhedral and quartz is observed in rounded and anhedral grains. Alkali feldspar has both pristine and turbid areas. The proportion of turbid feldspar in any one crystal is highly variable, but averages about 15–30%. Turbid areas have a brownish color in plane polarized light. Perthite texture is common, fine pristine perthites consist ~ 45 vol.%, and coarser patch perthites are dominant. Minor brown biotite occurs as euhedral flakes. Accessories are Mn-rich titanomagnetite, titanite, fluorite, zircon and apatite.

The perthite granite is distinguished from the syenogranite by its red color, smaller grain size (3–6 mm), absence of plagioclase and predominance of allotriomorphic and graphic texture. It consists of equant, anhedral perthite grains (~ 65%) and quartz (32%), with flakes of light brown biotite. Almost all alkali feldspar crystals are characterized by dense brown turbid patch perthite. The amount of accessory fluorite in the perthite granite is noticeably higher.

The Ab–Afs granite is mainly characterized by almost pure albite composition of plagioclase. Anhedral alkali feldspar grains, similar to those in perthite granite, constitute 41–65% of the rock volume. Albite forms prismatic crystals; its content ranges from a few to 20 vol.% (Table 1). In places, rare zoned plagioclase grains are also present. According to the IUGS classification (Le Maitre, 1989), both perthite granite and Ab–Afs granite are referred to as alkali-feldspar granite.

Overall, granites are fairly fresh. Alteration products in the syenogranite are mainly sericite in the core of zoned plagioclase crystals and chlorite that replaces biotite. In the alkali-feldspar granites, turbidity of alkali feldspar is extensively exhibited. Biotite is almost totally replaced by Fe-oxides and secondary mica that is compositionally intermediate between biotite and muscovite. Rare interstitial secondary muscovite is also present.

Porphyrytic varieties of the syenogranite, Ab–Afs granite, and perthite granite have the same modal composition and similar character of alteration as their coarse-grained equivalents. The proportion and size of quartz, feldspar, and rare biotite phenocrysts vary widely and the matrix is of hypidiomorphic, aplitic, granophyric, and micrographic texture.

5. Mineral chemistry

Perthitic alkali feldspar is the main mineral in the granites. According to estimates made by point counting in thin sections, the amount of the Ab exsolved phase in the alkali feldspar of the syenogranite is commonly 15–25 vol.% and does not exceed 40–45% (Fig. 3A). In the Ab–Afs granite the albite in perthite ranges mostly from 10 to 45 vol.%. The proportion of Ab phase in alkali feldspar of

Table 3
Chemical composition of granites from the Katharina pluton (wt.%, ppm)

Sample no.	D163	D165	D82	D85	D135	D26	D97	D54	D59	D93	D100	D43	D40
	Syenogranite						Albite–alkali feldspar granite					Perthite granite	
SiO_2	74.00	74.61	75.00	75.80	76.00	76.30	76.60	76.90	76.90	77.00	77.60	76.80	77.20
TiO_2	0.20	0.18	0.17	0.17	0.15	0.15	0.09	0.07	0.08	0.07	0.08	0.07	0.07
Al_2O_3	13.20	13.23	12.90	12.80	12.40	12.60	12.80	12.10	12.60	12.40	12.50	12.10	12.40
Fe_2O_3*	1.60	1.46	1.50	1.50	2.60	1.30	1.10	1.40	1.30	1.70	1.30	1.80	1.40
MnO	0.04	0.05	0.06	0.05	0.04	0.05	0.04	0.09	0.05	0.04	0.05	0.04	0.06
MgO	0.30	0.22	0.20	0.20	0.05	0.15	0.05	0.01	0.01	0.05	0.05	0.01	0.01
CaO	0.60	0.74	0.70	0.80	0.50	0.60	0.30	0.60	0.30	0.20	0.20	0.20	0.30
Na_2O	3.90	3.81	3.60	3.50	3.20	3.80	3.90	3.70	3.90	3.90	3.80	3.90	4.20
K_2O	5.00	4.95	5.00	5.00	5.10	4.40	4.70	4.20	4.40	4.50	4.20	4.30	4.00
P_20_5	0.05	0.48	0.05	0.05	0.10	0.05	0.05	0.05	0.05	0.05	0.05	0.05	0.05
LOI	0.50	0.07	0.30	0.40	0.40	0.30	0.40	0.60	0.30	0.30	0.30	0.30	0.50
Total	99.39	99.8	99.48	100.27	100.54	99.7	100	99.72	99.89	100.2	100.1	99.57	100.2
Rb	216	243	243	210	260	90	420	394	300	373	315	384	335
Sr	90	86	64	65	54	55	17	22	28	15	13	5	10
Ba	309	307	221	218	240	185	65	36	87	45	64	42	50
Nb	19	27	33	31	34	22	58	56	45	53	50	71	61
Ta	6	9	3	n.d.	n.d.	n.d.	n.d.	8	n.d.	4	n.d.	5	5
Th	27	26	23	n.d.	31	n.d.	40	31	30	30	n.d.	36	29
U	5	6	6	n.d.	4	n.d.	10	11	9	8	n.d.	9	10
Zr	175	176	184	180	140	120	150	156	145	105	140	184	149
Hf	6	6	6	n.d.	6	n.d.	8	8	7	6	n.d.	10	8
Y	28	35	41	39	26	13	76	67	50	61	52	83	75
Sc	2	3	4	n.d.	3	n.d.	2	1	2	4	n.d.	2	2
Ga	19	20	21	n.d.	n.d.	n.d.	n.d.	26	n.d.	25	n.d.	28	29
La	35.2	40.7	31.7	41	29	n.d.	19	26.3	26	17.6	24	28.5	26.3
Ce	78.8	86.7	71.5	81	68	n.d.	41	66.8	59	40.2	49	67.8	72.1
Pr	8.9	10.4	8.6	n.d.	n.d.	n.d.	n.d.	8.4	n.d.	6.5	n.d.	8.9	8.5
Nd	31.3	37	31.4	n.d.	27	n.d.	24	31	30	25.5	n.d.	31.9	31.4
Sm	6.4	7.6	6.6	n.d.	4.9	n.d.	8.1	8.3	7.3	7.4	n.d.	9.5	8.8
Eu	0.62	0.67	0.5	0.6	0.37	n.d.	0.11	0.14	0.21	0.18	0.1	0.07	0.08
Gd	5	6.1	5.5	n.d.	n.d.	n.d.	n.d.	8.6	n.d.	7.2	n.d.	9.8	8.5
Tb	0.82	1	0.92	n.d.	0.87	n.d.	1.3	1.6	1.4	1.4	n.d.	1.9	1.7
Dy	4.8	5.9	5.8	n.d.	n.d.	n.d.	n.d.	10.2	n.d.	8.4	n.d.	12.5	11
Ho	0.92	1.1	1.3	n.d.	n.d.	n.d.	n.d.	2.2	n.d.	1.8	n.d.	2.8	2.3
Er	2.8	3.3	3.6	n.d.	n.d.	n.d.	n.d.	6.5	n.d.	5.8	n.d.	7.5	6.8
Tm	0.48	0.63	0.58	n.d.	n.d.	n.d.	n.d.	1	n.d.	0.91	n.d.	1.2	1
Yb	3.2	4.1	3.9	5	3.7	n.d.	6	7.2	5	6.7	6	7.5	7.4
Lu	0.46	0.57	0.57	n.d.	0.68	n.d.	1.2	1.03	1	0.96	n.d.	1.1	1.03
(Na+K)/Al	0.9	0.88	0.88	0.87	0.87	0.87	0.9	0.88	0.89	0.91	0.86	0.91	0.91
Rb/Sr	2.4	2.8	3.8	3.2	4.8	1.6	24.7	17.9	10.7	24.9	24.2	76.8	33.5
K/Rb	192	169	171	198	163	406	93	88	122	100	111	93	99
Zr/Hf	30.7	29.8	29.2		23.7		20	19.5	19.6	17.8		18.2	18.4
La/Nb	1.85	1.51	0.96	1.32	0.85		0.33	0.47	0.58	0.33	0.48	0.4	0.43
Eu/Eu*	0.33	0.30	0.26		0.22		0.04	0.05	0.08	0.08		0.02	0.03

Fe_2O_3* = total Fe calculated as Fe_2O_3.

perthite granite varies widely, but its maximum frequency occurs at 45 to 65%. Both perthite and antiperthite are equally abundant.

Microprobe analysis showed significant difference in the composition of albite and K-feldspar phases in perthite grains from the syenogranite and alkali-feldspar granites (Fig. 3B and C). In the syenogranite the compositions of albite and K-feldspar phases show a large variation. The amount of *An* component in the albite phase ranges from 1 to 6.4%, and in the K-feldspar phase the *Ab* content varies within 11–13% in the majority of samples. In the alkali feldspar granite group, the K-feldspar phase of perthite is actually pure orthoclase, and in the albite phase the proportion of the *An* component is mostly less than 2%.

Plagioclase is present in the syenogranite and Ab–Afs granite. In the syenogranite the most abundant composition is An7–11; plagioclase with higher *An* up

to 15–20 mol% is found only in the cores of zoned crystals (Fig. 4). In the Ab–Afs granite, plagioclase is albite with *An* content ≤ 7%, mostly 1–3 mol%.

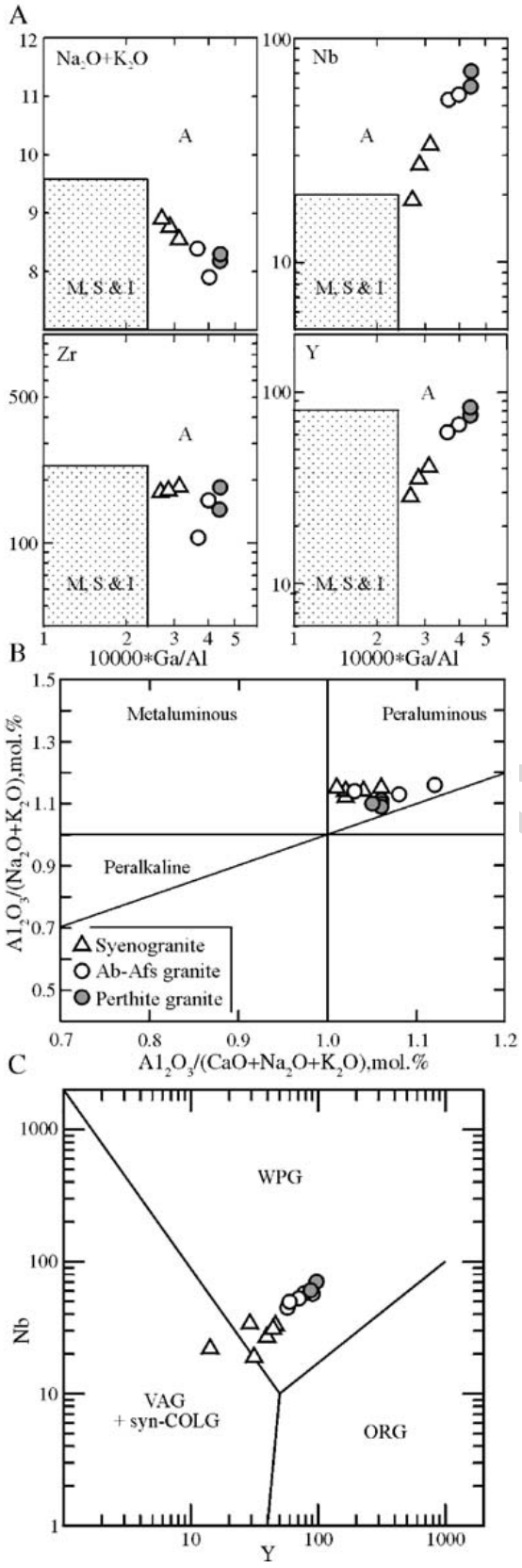

Biotite is the only mafic mineral in all types of granites. It is intermediate between annite and phlogopite, with 1.6–3.5 wt.% F (Table 2). Commonly biotite is altered to a various extent; relatively fresh biotite is preserved mainly in the syenogranite.

6. Geochemistry

Chemical compositions of representative samples are reported in Table 3 and plotted in Figs. 5–7. High agpaitic index *NK/A* ranging from 0.86 to 0.91 (Table 3) indicates that the granites of the pluton are alkaline (Liégeous and Black, 1987). It follows from classification diagrams (Fig. 5A and B) that all varieties of granites are referred to as mildly peraluminous A-type granite. On the Pearce et al. (1984) diagram (Fig. 5C), the Katharina granites plot in the 'within-plate' field. More precise geochemical discrimination is difficult since the granite compositions straddle the border between postorogenic and anorogenic (rift-related) A-type granites on diagrams suggested by Eby (1992).

In the silica-variation diagrams (Fig. 6), Ab–Afs and perthite granites form a single group with almost complete compositional overlap (the alkali-feldspar granite group). The syenogranite compositions represent a separate group that is distinctive by lower concentration of SiO_2, Rb, Y, Nb and higher content of CaO, Sr, K_2O, Ba, TiO_2 and MgO (Fig. 6). The Zr content is relatively low for A-type granites: in both groups it constitutes 120–180 ppm (Fig. 5A, Table 3).

The syenogranite and alkali-feldspar granites also differ in their REE patterns (Fig. 7). The syenogranite is LREE-enriched as reflected in La/Yb ratios of 7.8 to 10.9, whereas in the alkali-feldspar granites this value is only 2.6–5.2. The Eu/Eu* value in the syenogranite ranges from 0.22 to 0.33, and in alkali-feldspar granites it is significantly lower, 0.02–0.08 (Table 3). Compared to the Ab–Afs granite, the perthite granite is mildly enriched in REE and has lower Eu/Eu* value (Fig. 7).

The chemical characteristics indicate that the Ab–Afs granite and perthite granite are highly differentiated and share in many aspects the features of granites with the tetrad REE effect (e.g. Bau, 1996; Irber, 1999; Jahn

Fig. 5. Discrimination diagrams for the Katharina pluton granites. *A* = diagrams for the A-type granite. A, M, S and I = A-type, M-type, S-type and I-type granites; field boundaries from Whalen et al. (1987). *B* = $Al_2O_3/(CaO+Na_2O+K_2O)$ vs. $Al_2O_3/(Na_2O+K_2O)$, mol%; field boundaries from Maniar and Piccoli (1989). *C* = Y vs. Nb. WPG = within-plate granite, ORG = ocean-ridge granite, VAG = volcanic-arc granite, syn-COLG = syncollision granite; field boundaries from Pearce et al. (1984).

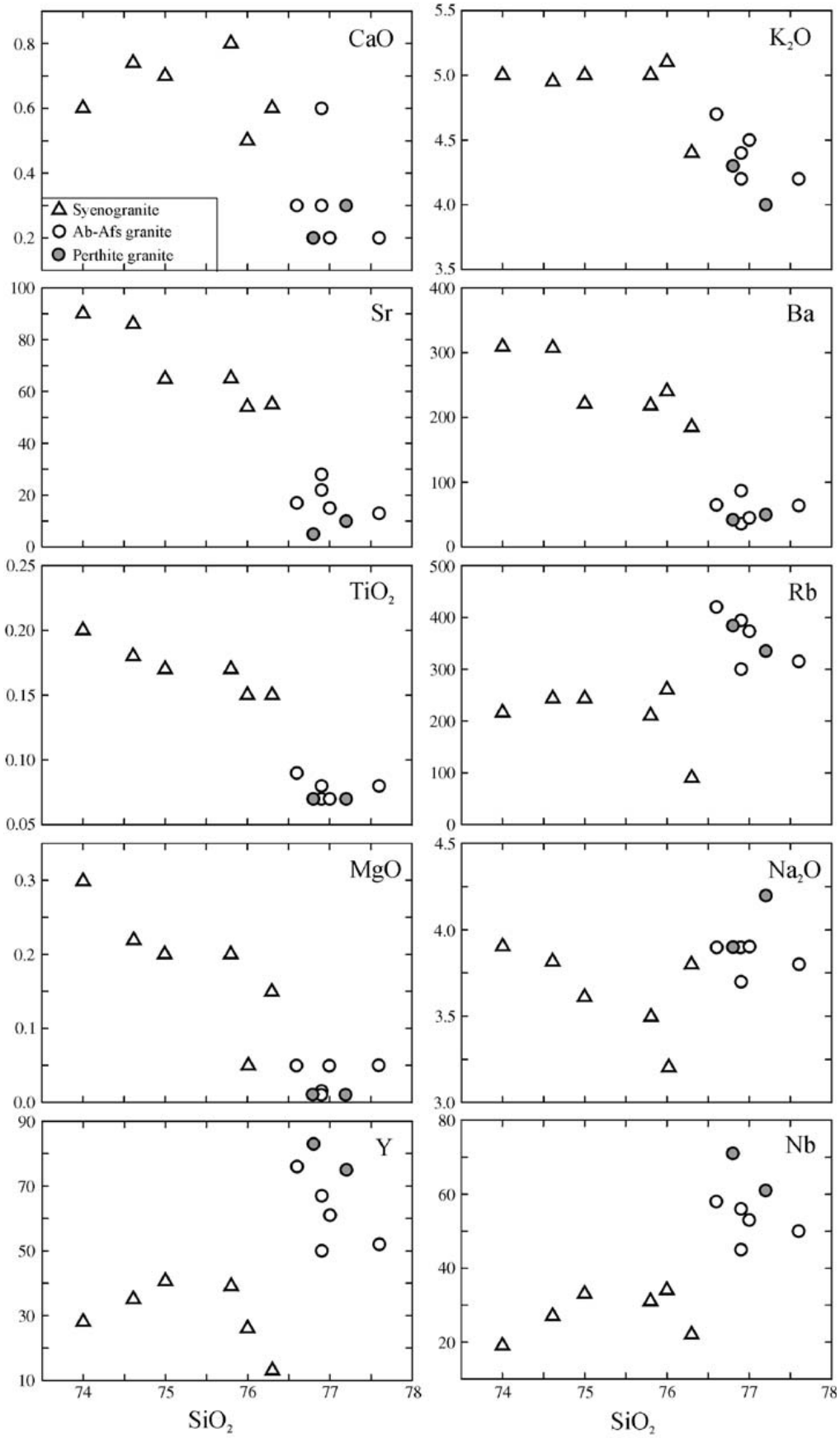

Fig. 6. Silica variation diagrams for the Katharina granites. Units are in wt.% (major elements) and ppm (trace elements).

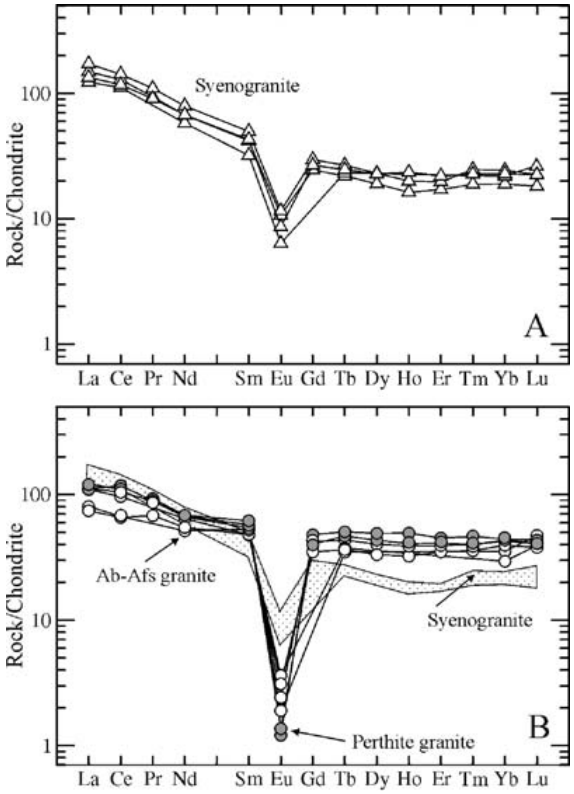

Fig. 7. Chondrite normalized REE patterns of the Katharina granites. Chondrite values from Sun and McDonough (1989).

et al., 2001; Jahn et al., 2004; Wu et al., 2004). Though the present alkali-feldspar granites do not show clear tetrad effect on REE, their non-CHARAC (charge-and-radius-controlled) behavior of certain elements is reflected by the high Rb/Sr (11–77), low K/Rb (90–120), low Zr/Hf (18–20), low La/Nb (0.33–2670.58), and very low Eu/Eu* (0.02–0.08). As emphasized by Jahn et al. (2001), the REE tetrad effect and non-CHARAC elemental behavior are most visible in late magmatic differentiates with strong hydrothermal interactions and occurs typically in highly evolved magmatic systems which are rich in H_2O, CO_2 and elements such as Li, B and F and/or Cl (e.g. London, 1986, 1987; Bau, 1996). This includes highly evolved leucogranites, pegmatites and mineralized granites.

7. Isotope characteristics

Oxygen isotopes. In terms of oxygen isotope ratios of quartz, the Katharina pluton is practically homogenous (Table 4). In ten samples collected from different lithologies and depths within the pluton, $\delta^{18}O$ (Qtz) varies over a narrow range of 8.03 to 8.55‰. No correlation was found between $\delta^{18}O$ (Qtz) values and either the altitude or type of granite sampled.

In contrast to the similarity in the oxygen isotope ratios of quartz, $\delta^{18}O$ (Afs) values clearly vary by lithology: in the syenogranite they range from 7.59 to 8.75‰, whereas in the alkali-feldspar granites $\delta^{18}O$ is markedly higher, at 9.14 to 9.66‰ (Table 4, Fig. 8). Oxygen isotope ratios of plagioclase are generally lower than those of alkali-feldspar (Table 4), however on the δ–δ diagrams (Fig. 8) they show similar grouping: $\delta^{18}O$ (Pl) in the syenogranite (7.58 to 7.86‰) is lower than in the Ab–Afs granite (8.31 to 9.12‰) regardless of $\delta^{18}O$ (Qtz). Experimentally determined equilibrium quartz–albite fractionations range from 0.58‰ at 1000 °C to 0.99 at 700 °C (Clayton et al., 1989). Thus the majority of the $\Delta^{18}O$ (Qtz–Afs) values measured in the Katharina pluton, which mostly range from 0 to −1.5‰, are clearly out of isotope equilibrium (Fig. 8). Feldspars are more susceptible than quartz to subsolidus oxygen isotope exchange. Therefore, a late or post-magmatic process that has significantly modified the oxygen isotope ratios of feldspars, but has left the $\delta^{18}O$ (Qtz) almost unchanged since the crystallization of the Katharina pluton is suggested. This process has affected the alkali feldspar granites more rigorously than the syenogranite (Fig. 8).

In the context of a systematic study of $^{18}O/^{16}O$ ratio in zircon from calc-alkaline and alkaline granitoid plutons in Sinai Peninsula, a composite separate of zircon was concentrated from six samples of the syenogranite collected within an area of 5 km^2 (D82–D87). Two fractions of zircon crystals, 63–100 μm and 100–200 μm, were analized. In duplicates the two size fractions of zircon have indistinguishable and homogeneous values: 5.87 and 5.80‰ for the coarse fraction and 5.86 and 5.75‰ for the fine fraction. This gives an average $\delta^{18}O$ (Zrn) value in the syenogranite of 5.82± 0.06‰. Since zircon best preserves magmatic isotope

Table 4
$\delta^{18}O$ values (‰, SMOW) of minerals from the Katharina pluton

Sample no./rock	Quartz	Plagioclase	Alkali feldspar
Syenogranite			
D111	8.48		8.75±0.14 (2)
D112	8.03	7.86	7.89
D130	8.55	7.58	8.33±0.07 (2)
D156	8.18	7.75	7.59
Ab–Afs granite			
D100 (Ab=20 vol.%)	8.47	8.31	9.54
D59 (Ab=11 vol.%)	8.34	9.12	9.64
D79 (Ab=6 vol.%)	8.21		9.14
Perthite granite			
D45	8.17		9.19
D46	8.27		9.66
D48	8.15		9.17

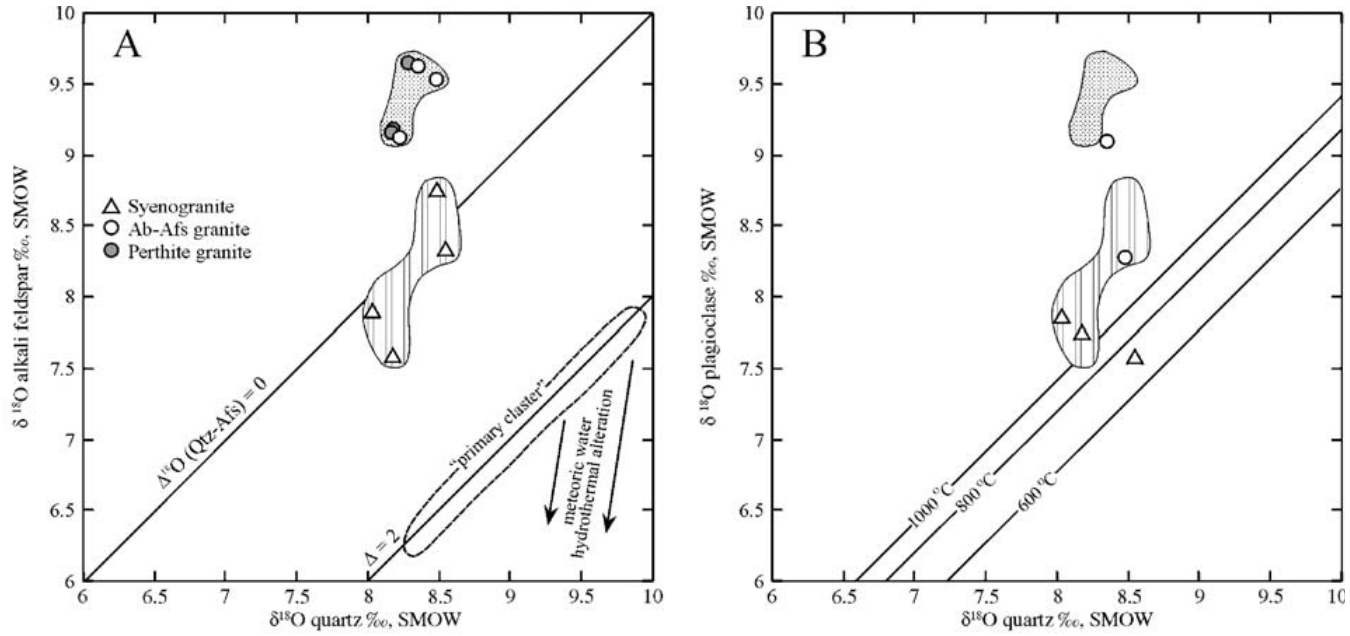

Fig. 8. δ–δ diagrams for the Katharina granites: quartz–alkali feldspar (A) and quartz–plagioclase (B). Fields from A are shown in B for comparison. The "primary cluster" field along $\Delta^{18}O$ (Qtz–Afs)=2‰ in A includes granite samples from the Idaho Batholith that have no apparent evidence for hydrothermal alteration. Arrows show the trend formed by rocks from the Idaho Batholith that were hydrothermally altered by meteoric water (Criss and Taylor, 1983). Isotherms in B are shown for equilibrium Qtz–Ab fractionations at 1000, 800 and 600 °C as experimentally determined by Clayton et al. (1989).

ratios, its $\delta^{18}O$ value is a powerful tracer for the origin of magma (Valley et al., 1994, 2005). The $\delta^{18}O$ (Zrn) value of the syenogranite only mildly exceeds the oxygen isotope range of mantle zircon (5.3±0.3; Valley, 2003). The origin of the Katharina granitic magma should thus be sought in mantle-derived sources, whereas upper crustal contribution remains minimal. The fractionation between the average $\delta^{18}O$ values of quartz and zircon in the syenogranite, ~2.5‰, is slightly higher than predicted by isotope equilibrium at 800 °C (~2.3‰, Vallley et al., 2003) and suggests small modification of the magmatic $\delta^{18}O$ (Qtz) by closed-system exchange during post-crystallization cooling.

Rb–Sr and Sm–Nd data were obtained for five samples, of them two samples from the Katharina pluton and three samples from the ring dikes (Table 5). In addition, Bielski (1982) carried out Rb–Sr isotope analysis of two samples from syenogranite and two samples from alkali-feldspar granite collected by one of the authors (M. Eyal). These results are also included in the Table 5 and isochron is recalculated. Since accuracy of data obtained more than 20 years apart is different, three isochrons were calculated, separately, for the authors' data, Bielski's data and the whole set of data (Fig. 9). All three isochrons yielded actually the same age of about 590 Ma, with $(^{87}Sr/^{86}Sr)_o$=0.7022±0.0064 calculated for the whole set of samples. The Rb–Sr age is in good agreement with U–Pb age of zircon from the Katharina syenogranite, 583±5.6 Ma, MSWD=1.8 (unpublished data obtained by Y. Beeri in the NORDSIM Facility, Swedish Museum of National History, Stockholm).

The ε_{Nd} (T) values are +3.6 and +3.9 in plutonic rocks and vary from +4.5 to+5.5 in the ring dike rocks. All rock types have rather young depleted-mantle-based model age of about 900–1000 Ma assuming two-stage evolution.

The Rb–Sr age of the Katharina pluton and the Katharina Ring Complex as a whole is identical (within the uncertainly limits) to the ages of other Late Pan-African A-type granites that are abundant in the Arabian–Nubian Shield. Ages of A-type granite plutons are 587±11 and 600±11 Ma in Egypt and Saudi Arabia (Baurbon et al., 1976; Stern and Hedge, 1985; Moghazi, 1999), 608 Ma in Jordan (Jarrar et al., 1983) and 610±10 Ma in southern Israel (Beyth et al., 1994).

The ε_{Nd} (T) values of the syenogranite from the Kathatina pluton are similar to those in alkaline granite from the Timna Complex in southern Israel (+3.9, Beyth et al., 1994) and noticeably lower than in monzogranite from the Gebel El–Urf area, eastern Desert, Egypt (+5.2 to +5.8, Moghazi, 1999). However, ε_{Nd} (T) of silicic rocks from the Katharina ring dikes overlap the latter values.

Table 5
Rb–Sr and Sm–Nd isotope data of rocks from the Katharina Ring Complex

Sample no.	Rock	Rb (ppm)	Sr (ppm)	$^{87}Rb/^{86}Sr$	$^{87}Sr/^{86}Sr$	±2σ	[Sm] (ppm)	[Nd] (ppm)	$^{147}Sm/^{144}Nd$	$^{143}Nd/^{144}Nd$	±2σ	ε_{Nd} (0)	εNd (T)	f (Sm/Nd)	TDM-1 (Ma)	TDM-2 (Ma)
1. D163	Syenogranite	220.5	91.29	7.013	0.758037	8	6.34	32.57	0.1177	0.512519	3	−2.3	3.6	−0.40	1002	1010
2. D165	Syenogranite	238.3	86.75	7.983	0.767362	8	7.26	36.33	0.1208	0.512546	3	−1.8	3.9	−0.39	991	971
3. ME-111*	Syenogranite	229	84.9	7.67	0.7677											
4. ME-132*	Syenogranite	203	127	4.57	0.7429											
5. ME-80*	Alkali-feldspar granite	324	24.2	39	1.036											
6. ME-127*	Alkali-feldspar granite	237	27.7	24.6	0.9099											
7. IL-66	Qtz monzonite porphyry	53.8	396.9	0.367	0.706085	7	10.97	62.42	0.1062	0.512571	3	−1.3	5.5	−0.46	822	911
8. IL-161	Qtz syenite porphyry	99.6	305.3	0.943	0.710773	7	12.08	72.82	0.1003	0.512503	3	−2.6	4.6	−0.49	870	1012
9. AG-32	Peralkaline granite porphyry	204.9	8.96	69.85	1.291379	10	12.17	63.49	0.1159	0.512558	3	−1.6	4.5	−0.41	923	945

Samples IL-66, IL-161 and AG-32 from the ring dikes; the rest are from the pluton.
*=after Bielski (1982). Values of 2σ vary from 16 to 39. Blanks: Sr=55 ng, Nd=25 ng. NBS 987 (3 runs) — 0.710236±7; 0.710226±6; 0.710244±7 (average=0.710235). Sr isotope ratios have been adjusted upward relative to NBS-987=0.710250. Ames Nd Rennes standard (2 runs): 0.511964±3; 0.511963±3. J Ndi standard (1 run): 0.512110±3. ε_{Nd} (T) values were calculated based on T=590 Ma.

8. Discussion

It was shown in the foregoing sections that the Katharina pluton consists of two main rock varieties, syenogranite that makes up the bulk of the pluton, and alkali-feldspar granites occupying its upper part. The two rock types are clearly distinguished in modal composition, mineral chemistry, whole rock chemical composition and oxygen isotope ratios of feldspars. The alkali-feldspar granites are, in turn, divided into two subzones, the uppermost perthite granite and the lower Ab–Afs granite (Fig. 2). Therefore the problem of the pluton zoning is considered in two respects: (1) generation of the alkali-feldspar granite and (2) formation of the perthite granite and Ab–Afs granite subzones.

8.1. Origin of the alkali-feldspar granite

8.1.1. None-hydrothermal origin

The fact that alkali-feldspar granites are located in the uppermost part of the pluton and have a gradational contact with subjacent syenogranite suggests that the vertical zoning was formed either in the course of evolution of a voluminous batch of magma or resulted from hydrothermal alteration of the syenogranite in the upper part of the pluton.

The available data suggest that the alkali-feldspar granite zone had been produced at the magmatic stage. The geological evidence in favor of this viewpoint is the predominance of magmatic textures in all three types of granites. Particularly convincing is the presence of porphyritic varieties of alkali-feldspar granites in the pluton margins. The porphyritic rocks have the same modal composition as their coarse-grained equivalents from the interior of the pluton. Granophyric, aplitic and micrographic matrix point to crystallization of feldspar–quartz intergrowths from cotectic melts.

From the standpoint of a hydrothermal alteration model, the Ab–Afs granite should be considered as an intermediate product of metasomatic alteration of the syenogranite. This is defined by its stratigraphic position and transitional modal composition exhibited in systematic decrease of plagioclase proportion from 20 vol.% to almost zero going from the contact with the syenogranite upward to the perthite granite. However, the whole-rock composition and mineral chemistry do not support the transitional nature of this rock type. As seen in Figs. 6 and 7, the compositions of the Ab–Afs granite differ significantly from the syenogranite, but overlap those of the perthite granite. Uniform composition of plagioclase in the Ab–Afs granite, despite the wide range of its proportion (Fig. 4), is another piece of evidence that

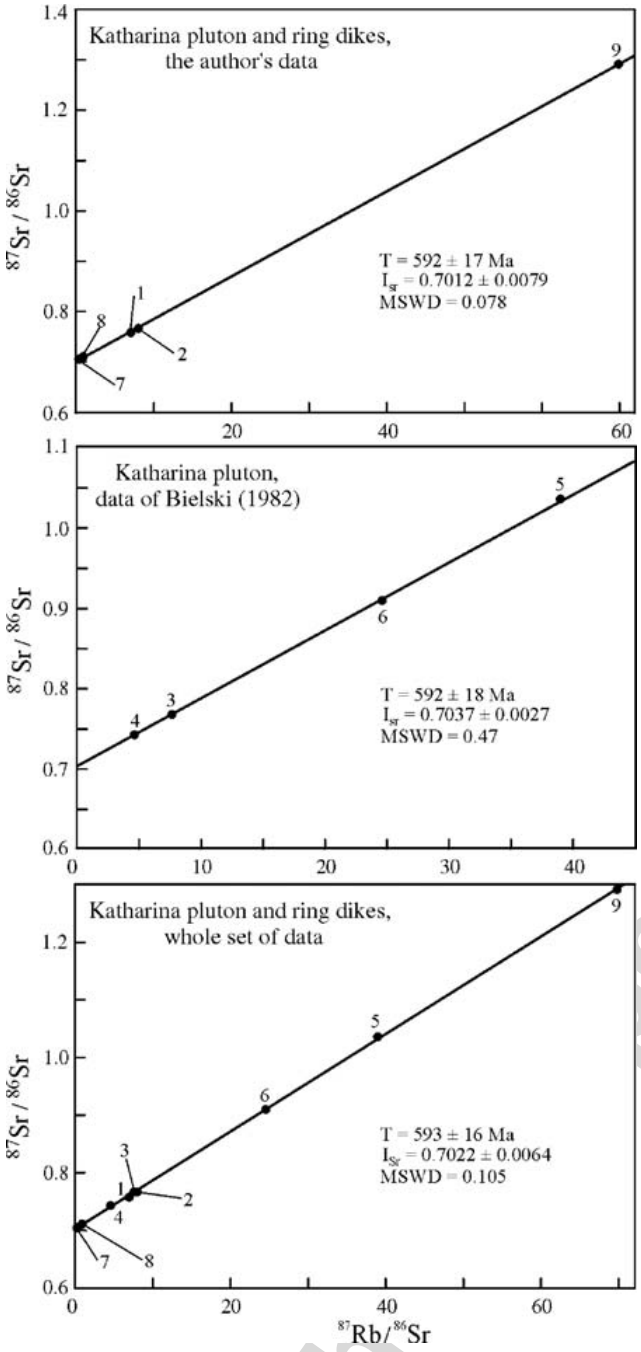

Fig. 9. Rb–Sr isochron diagrams of plutonic and ring dike rocks from the Katharina Ring Complex. Sample numbers as in Table 5. For Bielski's data, input errors are 2% for $^{87}Rb/^{86}Sr$, 0.2% for $^{87}Sr/^{86}Sr$; the errors quoted in age represent ±1δ.

argues against the formation of this rock type by hydrothermal alteration of the syenogranite. The insignificant role of metasomatic processes is consistent with the fact that the country rocks intruded by the Ab–Afs granite do not show any evidence of metasomatic effects.

The oxygen isotope ratios of quartz also advocate magmatic rather than hydrothermal origin of the alkali-feldspar granites. Relatively low $\delta^{18}O$ values of about 8.1–8.5‰ are typical of quartz from all three types of granites (Table 4), whereas in epizonal granites affected by hydrothermal alteration some shift in $\delta^{18}O$ (Qtz) relative to igneous values should be expected (King et al., 1997). Therefore, it is unlikely that extensive metasomatic alteration that has culminated in the transformation of syenogranite into perthite granite did not affect the oxygen isotope ratios of quartz. The Rb–Sr isotope system also does not exhibit evidence of noticeable disturbance. This follows from Fig. 9 demonstrating that alkali-feldspar granite samples are well in line with the isochron calculated for the Katharina Ring Complex as a whole. The hydrothermal alteration model is also in conflict with available geochemical data. It was shown (Orville, 1963) that the proportion of K to (K+Na) in the vapor phase that coexists with two alkali feldspars decreases with falling temperature. This means that the high-temperature fluid that formed in the course of the pluton crystallization and ascended to its cooler roof zone should have caused enrichment of this zone in K-feldspar, i.e. in K_2O. However, the real picture is opposite (Fig. 6). Also the hydrothermal alteration model cannot account for a number of other geochemical features of the alkali-feldspar granites that distinguish them from the syenogranite (Fig. 6, Table 3): (1) opposite behavior of K and Ba with respect to Rb; (2) increase in Nb, Y and U; (3) enrichment of the alkali-feldspar granite in SiO_2 (and modal quartz). The non-CHARAC behavior of certain elements is known to occur still in the end-stage magmatic evolution where interaction of magma and fluids resulted in REE tetrad effect and atypical elemental relations.

8.1.2. Origin by crystal fractionation

Notwithstanding, the geochemical data are consistent with magmatic origin of the alkali-feldspar granites suggesting that the most likely process of their generation was fractional crystallization. Efficient depletion of the residual melt in Ca and Sr can be readily provided by separation of oligoclase from the syenogranite magma. Likewise, fractionation of K-rich alkali feldspar crystals, which is characteristic of subliquidus stages of the granite magma crystallization (Tuttle and Bowen, 1958; Johannes and Holtz, 1996), should result in the impoverishment of the residual melt in K and Ba, with simultaneous increase in Rb (Fig. 6). Fractionation of the two feldspars would also increase the negative Eu anomaly (Fig. 7). Decrease of MgO and TiO_2 contents in the alkali-feldspar granites suggests fractionation, along with feldspars, of mafic and possibly ore minerals.

Numerical modeling of crystal fractionation from the syenogranite magma that resulted in the formation of the alkali-feldspar granite residuum was performed using a

least-square approximation (GPP program, Terra Softa Inc., 1985) for nine major oxides. Calculation was made based on the average composition of the syenogranite as a parental melt and the average alkali-feldspar granite as a daughter melt. The compositions of rock-forming minerals from the syenogranite, plagioclase (An_{11}), K-rich alkali feldspar (Or_{80}) and biotite from sample D10 (Table 2) were used; the apatite composition was taken from Cox et al. (1980, Appendix 5). The results are presented in Table 6. The observed and calculated daughter melt compositions fit well. Slight discrepancy in MgO and TiO_2 can be accounted for by very low content of these oxides in granites. It follows from Table 6 that five minerals could be subjected to fractionation, of them plagioclase, K-feldspar and quartz constitute more than 90%. The degree of crystallization is ~ 50 wt.%. The major element modeling was tested by Rb, Ba and Sr, which reside dominantly in major mineral phases. Their redistribution in the residual melt is controlled primarily by fractionation of feldspars (Bea, 1996). A test for Sm, Eu and Tb (owing to the lack of distribution coefficients for Gd) was made since it provides calculation of Eu/Eu∗ value that exhibits the role of feldspar fractionation and depends little on the amount of REE contributed by accessory minerals. Testing was performed using the method suggesting by De Paolo (1981). It is seen from Table 6 that the test also gave a satisfactory match between the calculated and observed values.

Table 6
Results of least-square modelling of the syenogranite magma fractional crystallization, with the trace element testing

	Parent syenogranite, average	Daughter Afs granite, average	
		Observed	Calculated
SiO_2	75.81	77.48	77.31
TiO_2	0.17	0.08	0.19
Al_2O_3	12.94	12.49	12.46
FeO*	1.50	1.29	1.26
MgO	0.19	0.03	0.18
CaO	0.66	0.30	0.33
Na_2O	3.66	3.92	3.90
K_2O	4.94	4.36	4.35
P_2O_5	0.13	0.05	0.01
Fractionating minerals, wt.%	Alkali feldspar		17.1
	Plagioclase		12.7
	Quartz		16.1
	Biotite		3.1
	Apatite		0.3
Residual melt, wt.%			50.7
Sum residuals squared			0.07
	Trace element testing		
Rb	210	360	315
Ba	242	56	62
Sr	69	16	19
Sm	6.40	8.2	8.3
Eu	0.54	0.13	0.2
Tb	0.90	1.6	1.2
Eu/Eu*	0.28	0.05	0.07

(1) Major elements are recalculated to total = 100% volatile free and total Fe as FeO*. (2) Sources of partition coefficient values: Stix and Gorton, 1990 (Afs); Nash and Crecraft, 1985 (Pl, Qtz, Bt); Arth, 1976 (Ap). Partition coefficients for Tb in Pl and Ap are obtained by interpolation.

Although the dominant role of fractional crystallization is supported by convincing pieces of evidence and mass-balance calculations, a number of geochemical traits cannot be accounted for by crystal fractionation. This concerns noticeable enrichment in HREE relative to LREE in the alkali-feldspar granites (Fig. 7) and abrupt increase in Nb, Y, U over a restricted range of SiO_2 (Fig. 6, Table 3). It is worth noting that similar geochemical features were reported in Late Pan-African A-type granites located in the adjacent areas of the Northern Desert, Egypt. Moghazi and co-authors (Moghazi et al., 1998, 1999) have shown that the magma that produced these granites was enriched in F. They drew attention to experimental data demonstrating that F-rich fluid can cause HREE and HFSE enrichments due to F complexing in the late stages of evolution of a granitic melt (Dingwell, 1988; Ponader and Brown, 1989; Rogers and Satterfield, 1994). This interpretation seems appropriate for the Katharina alkali-feldspar granites. In these granites evidence of extensive fluid–magma interaction is clear (see Sections 6 and 7). Enrichment in F is exhibited by abundant fluorite and by high, ~ 3 wt.%, F contents in biotite both from syenogranite and alkali-feldspar granite (Table 2). Hence, it is likely that some geochemical features of alkali-feldspar granites were significantly affected by F complexes at the final stages of crystallization.

8.2. Possible model for residual melt extraction

The estimate of crystal–melt proportion enables us to propose a mechanism that governed efficient extraction of the highly viscous residual silicic melt from the magmatic "mush". The calculated value of the degree of crystallization, about 50 wt.%, is close to the rigid percolation threshold (RPT) or "critical melt percentage" in felsic magma (Van der Molen and Peterson, 1979; Vigneresse et al., 1996). According to these authors, when the proportion of crystal phase achieves the RPT value (about 55%), the crystals construct a rigid skeleton in the magma; clusters of crystals can sustain stress, whereas the liquid fraction can still flow. At this stage residual melt may flow pervasively through pore

space or fracture network (e.g. Brown and Solar, 1999; Weinberg, 1999; Leitch and Weinberg, 2002).

The granite magma that formed the Katharina pluton was emplaced and crystallized under a volcanic roof that was hardly more than 2–3 km thick. When the proportion of crystals became more than 55–60%, only residual melt of alkali-feldspar granite composition could flow upwards. It is likely that the main driving force of such flow was fracturing of the roof. According to Bons et al. (2004), deformation aids melt extraction much more efficiently than buoyancy of melt, so that segregation and accumulation of residual magma could readily occur in a tectonically unstable system. The residual melt flow to the roof resulted in formation of alkali-feldspar granite zone with a dome-like projection in the vicinity of Gebel Bab (Figs. 1 and 2). Gradational contact with the subjacent syenogranite is accounted for by the fact that the syenogranite still contained significant proportion of liquid phase at the time of the upper zone formation.

8.3. Origin of subzones in the alkali-feldspar granites

The perthite granite and the Ab–Afs granite form two distinct subzones with a gradational contact. Chemical and oxygen isotope similarities of both varieties of granite (Figs. 6–8; Tables 4 and 5) allow us to assume that they were derived from the same parent magma. Judging from the modal composition, perthite granite and Ab–Afs granite correspond to hypersolvus and subsolvus types, respectively. It is known that the type of granite strongly depends on the water pressure during crystallization: hypersolvus rocks crystallize from magma with low water fugacity, whereas for subsolvus (two feldspar) granite to form, magma should be enriched in water. In pure haplogranite system the critical P_{H2O} must be $\geq$3.5–4 kbar (Yoder et al., 1957; Tuttle and Bowen, 1958). However, it was shown that crystallization of two separate feldspars occurs at lower P_{H2O} when the system contains An and fluorine. James and Hamiltin (1969) observed two feldspars in the system $(Ab–Or–Qtz)_{97}An_3$ at $P_{H2O}=1$ kbar and $T=720$ °C. According to experimental data reported by Kovalenko (1978), crystallization of low-Ca granite system (0.11–0.42 wt.% CaO) resulted in formation of two feldspars at $P_{H2O}=1$ kbar when the fluorine concentration was $\geq$0.1 wt.%. Based on these data, the following hypothesis for the formation of the two subzones in the Katharina pluton is suggested.

The parent syenogranite magma, like most A-type magmas, was probably water-undersaturated and contained about 2–3 wt.% H_2O (Reyf and Bazheev, 1985; Clemens et al., 1986; Whalen et al., 1987; Vielzeuf et al., 1990; Litvinovsky et al., 2000, 2002). Since the inferred residual melt that produced the alkali-feldspar granites was separated from a magmatic syenogranitic "mush" that contained >50% crystals (Table 6), its water concentration should increase to 4–6 wt.%, which is above the water saturation value in silicic magma at the depth of crystallization of about 2–3 km, i.e. at pressure of less than 1 kbar (Johannes and Holtz, 1996; Holtz et al., 2001). When the evolved, water-saturated melt was emplaced under the volcanic roof, its crystallization started from formation of hypersolvus perthite granite. However, fluid flux to the upper part of the pluton continued, leading to P_{H2O} increase in the magma immediately below the upper perthite granite zone and resulting in crystallization of two-feldspar granite. The water pressure increase should not be dramatic since the granitic melt contained about 1.0–1.5 mol% An (Table 3) and was noticeably enriched in F, as indicated by the abundance of accessory fluorite in alkali-feldspar granite and the presence of ~ 3 wt.% F in biotite (Table 2). According to the Parsons' diagram (Fig. 1 in Parsons, 1978), crystallization of the alkali-feldspar granite magma leads to formation of subsolvus granite at water pressure that only slightly exceeded 1 kbar. The aqueous fluid could not escape efficiently from the viscous granite magma, therefore enhanced P_{H2O} retained longer at some depth and caused crystallization of subsolvus granite with varying proportion of albite crystals.

8.4. Evidence for subsolvus fluid–rock interaction

Extensive subsolvus fluid–rock interaction in the Katharina pluton is indicated by exsolution textures in alkali feldspars and specific oxygen isotope characteristics of feldspars and quartz.

Exsolution textures exhibit a great diversity in morphology, including abundant coarsening of perthites and widespread turbidity in alkali feldspar crystals. Structural rearrangement of alkali-feldspars is characteristic of all types of the Katharina granites, but more so in the upper part of the pluton. In the syenogranite about 45 vol.% of pristine fine perthites have been retained, and the proportion of turbid alkali feldspar ranges from 15 to 30%. In the alkali-feldspar granites, however, coarse patch perthites dominate, making up about 80–90%, and almost all alkali feldspar is turbid. In these granites the structural rearrangement of the perthite was accompanied by formation of pure albite lamellae and pure host orthoclase (Fig. 3B and C), which is not typical for pristine perthite (Tuttle and Bowen, 1958;

Parsons, 1978). In contrast, albite phase in perthites from the syenogranite contains up to 5–6% *An*, and *Ab* component attains 11–17% in orthoclase.

Several studies showed that abundance of exsolution textures in alkali feldspar indicates extensive structural rearrangement of magmatic alkali feldspar at low temperatures ≤400 °C (e.g. Parsons, 1978; Brown and Parsons, 1989; Worden et al., 1990; Lee et al., 1995; Walker et al., 1995). The turbidity in alkali feldspars stems from numerous tiny, 1–2 μm, micropores that point to recrystallization driven by infiltration of aqueous fluid. According to the data of Parsons and associates (see above refs.), coarse patch perthite in subsolvus feldspars developed isochemically by water-impelled dissolution and reprecipitation. Isochemical recrystallization of perthite accounts for the narrow compositional range of the alkali-feldspar granites (Fig. 7). This suggests that in the course of recrystallization the system remained closed. Closed-system behavior is also supported by the well-established Rb–Sr isochrons constructed for the Katharina Ring Complex including samples from the alkali-feldspar granites. Thus the Rb–Sr isotope system was not disturbed by sub-solvus interaction with fluids (Fig. 9). It follows that the main proportion of water that caused the feldspar recrystallization should come from the granite magma itself. The dominance of exsolution and alteration textures of perthite grains from the alkali-feldspar granites suggests that fluid phase was present in the upper part of the pluton for a long time after its emplacement and crystallization.

Quartz–alkali feldspar oxygen isotope fractionations further constrain the origin of fluids during the late subsolvus alteration of the Katharina pluton (Fig. 8). Measured fractionations between magmatic quartz and alkali feldspar [$\Delta^{18}O$ (Qtz–Afs)] and between quartz and plagioclase in granites are typically about 1 to 1.5‰ and 1.5 to 2.5‰, respectively (Taylor, 1977). These are slightly larger than the experimentally determined equilibrium $\Delta^{18}O$ (Qtz–Afs) at 800 °C (Clayton et al., 1989) and probably reflect inter-mineral subsolidus oxygen exchange of quartz down to 600 °C and feldspar–fluid exchange down to 350 °C during cooling of plutonic rocks (Valley, 2001). None of the measured $\Delta^{18}O$ values in the Katharina pluton plot in the expected range for cooling granitic plutons at any temperature (Fig. 8): $\Delta^{18}O$ (Qtz–Afs) in the syenogranite are 0.6 to −0.3‰, whereas fractionations in the alkali-feldspar granites are even lower and more negative: −0.9 to −1.4‰. The variation in fractionations reflect the ~ 1‰ higher $\delta^{18}O$ (Afs) values in the alkali-feldspar granite relative to the syenogranite. This difference suggests that the water–rock interaction responsible for feldspar recrystallization and higher abundance of patch perthite in the upper part of the pluton has modified the oxygen isotope ratio of feldspar to a greater extent in the alkali feldspar granite than in the syenogranite. However, the negative, non-equilibrium $\Delta^{18}O$ (Qtz–Afs) values (about −1‰) in the alkali-feldspar granites seen on the $\delta^{18}O$ (Afs) vs. $\delta^{18}O$ (Qtz) diagram (Fig. 8) rule out massive hydrothermal alteration by circulating heated meteoric water. Oxygen exchange with hot meteoric water would instead appreciably decrease the isotopic ratio of feldspar relative to quartz to form highly positive quartz–alkali feldspar fractionations (Criss and Taylor, 1983, 1986). Water in exchange equilibrium with alkali-feldspar ($\delta^{18}O$=9.7‰) at 400 °C, the assumed temperature of formation of the patch perthite, would have $\delta^{18}O$=6.2‰ (O'Neil and Taylor, 1967). The most feasible source for such ^{18}O-rich water is the granitic magma itself. Water in equilibrium with quartz ($\delta^{18}O$=8 to 8.5‰) of the crystallizing syenogranite magma (~ 700 °C) at the deeper part of the Katharina pluton would acquire $\delta^{18}O$ of ~ 7.5 to 8‰ (O'Neil et al., 1969; Chiba et al., 1989). If such H_2O migrated upward from the syenogranite zone, diluted by small amount of meteoric water infiltrating through the volcanic roof, and came into contact with the alkali-feldspar granites at ~ 400 °C, it could produce the isotope shifts observed in the upper part of the pluton.

8.5. Provenance of the syenogranite magma

To explain the origin of A-type granites, a number of petrogenetic models have been proposed in which crustal, mantle-derived or mixed sources were suggested. Numerous Sm–Nd and Rb–Sr isotope data obtained during the last decade suggest that many silicic magmas of this type were produced from sources in which mantle-derived material was dominant (e.g. Turner et al., 1992; Whalen et al., 1996; Jahn et al., 2000; Bonin, 2004; Jahn et al., 2004). The isotope data on the Katharina pluton support this conclusion.

The $\delta^{18}O$ values of zircon 5.82±0.06 (Table 4) is only slightly higher than $\delta^{18}O$ range of zircon in the mantle (Valley, 2003). This suggests dominance of the mantle component in the source region. The oxygen isotope ratios of quartz in the Katharina pluton were left unaffected by late deuteric alteration and thus roughly retain the pristine magmatic values. Assuming that $\delta^{18}O$ (Qtz) is ~ 1 to 1.5‰ higher than the granite whole rock value, the Katharina pluton is within the range of the "intermediate ^{18}O (WR) group" (7.0 to 7.7‰) of Taylor (1968, 1978). Such values indicate no crustal contribution

to the granitic magma and support a mantle-derived origin for the Katharina pluton (Taylor and Sheppard, 1986).

Low initial $^{87}Sr/^{86}Sr$ values (0.7022), positive ε_{Nd} (T) values ranging from +3.6 to +5.5 in the Katharina Ring Complex (Table 5), and mantle-like $\delta^{18}O$ (Zrn) in syenogranite point to 'juvenile' character and suggest that the silicic magma was derived either by partial melting of juvenile crust or by differentiation of mantle-derived magma. It follows from data in Table 5 and Fig. 9 that the crystallization age (~ 590 Ma) and Nd model age TDM2 (900–1000 Ma) differ significantly. Since TDM2 corresponds to the time when the source of granite magma has been isolated from the mantle source (De Paolo et al., 1991), the observed difference suggests later thermal reworking of the mantle source material and possibly admixture of crustal component. This means that the ε_{Nd} (T) values calculated for granites cannot be interpreted straightforward as indication of mildly depleted mantle source of granite (Arndt and Goldstein, 1987). However, these values attest that the granites from the Katharina pluton contain >>50% of mantle (or young juvenile crust) component. Similar models were suggested for other A-type granites of the Arabian–Nubian Shield (Stern and Hedge, 1985; Beyth et al., 1994; Moghazi, 1999).

No matter where the source regions of the alkali granite magmas were located, either in the young 'juvenile' crust or in the metasomatized mantle, negative Nb anomaly like the one shown in Primitive Mantle-normalized spidergrams of the Katharina pluton should be expected (Fig. 10). However, the very low Ba, Sr and Eu abundances require an advanced fractionation of feldspars in upper crustal conditions. Data on the provenance of the Katharina pluton are in full agreement with the notion of the juvenile nature of the Arabian–Nubian Shield and high rate of crustal growth in the Neoproterozoic (e.g. Bentor, 1985; Stern and Kröner, 1993; Stern, 1994; Stein and Goldstein, 1996).

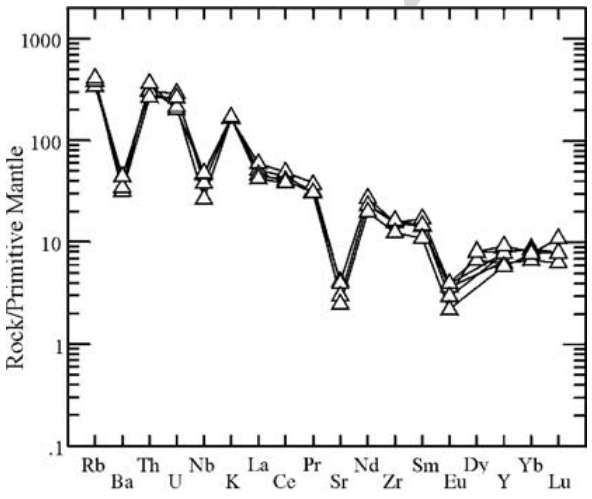

Fig. 10. Primitive mantle-normalized multi-element diagram for syenogranite from the Katharina pluton. PM values from Sun and McDonough (1989).

9. Conclusion

The Katharina pluton, characterized by vertical zoning from syenogranite to alkali-feldspar granites, was emplaced at ~ 590 Ma. It represents post-orogenic A-type granite plutons abundant throughout the Arabian–Nubian Shield.

The vertical zoning in the pluton was caused by fractional crystallization of the syenogranite magma. A water-saturated residual melt of alkali-feldspar granite composition was separated at extent of crystallization of >50 wt.%, which approximates the rigid percolation threshold for silicic melts. Its separation proceeded by upward flow through the rigid solid particle clusters. Crystallization of the evolved melt started with formation of upper hypersolvus granite zone immediately under the roof. Fluid influx from the inner part of the pluton to its apical part persisted and caused increase of water pressure in the magma below the perthite granite; this led to crystallization of subsolvus Ab–Afs granite. Owing to the presence of F and Ca in the melt, P_{H2O} should have increased to slightly more than 1 kbar to allow subsolvus crystallization. The Katharina pluton can be considered as an explicit example demonstrating that fractional crystallization of syenogranite magma could result in formation of alkali-feldspar granite.

Low initial $^{87}Sr/^{86}Sr$ values (0.7022), positive ε_{Nd} (T) values ranging from +3.6 to +5.5 in the Katharina Ring Complex (Table 5), and almost mantle-like $\delta^{18}O$ values of zircon (5.82‰) attest to generation of silicic melt from a mantle or 'juvenile' crustal source, which is typical of the rocks making up most of the Arabian–Nubian shield.

Acknowledgements

The study was supported by the Israel Science Foundation, grant #142/02, by the Ministry of National Infrastructure and Energy, Israel, grant #23-17-04, and by the National Science Council (NSC), Taiwan, grants NSC93-2116-M-001-025, NSC94-2116-M-001-021, NSC94-2752-M-002-010-PAE. We thank David Kosashvili for thin section preparation, Elad Yizraeli for help with the electron microprobe analysis, and Mike Spicuzza (University of Wisconsin, USA) for help in oxygen isotope analysis. Authors are indebted to the editor S. Foley and anonymous reviewers for constructive remarks and discussion that have greatly improved an earlier version of the manuscript.

References

Arndt, N.T., Goldstein, I.V., 1987. Use and abuse of crust-formation ages. Geology 15, 893–895.

Arth, J.G., 1976. Behaviour of trace elements during magmatic processes — a summary of theoretical models and their applications. J. Res. U.S. Geol. Surv. 4, 41–47.

Bau, M., 1996. Controls on the fractionation of isovalent trace elements in magmatic and aqueous system: evidence from Y/Ho, Zr/Hf, and lanthanide tetrad effect. Contrib. Mineral. Petrol. 123, 323–333.

Baurbon, J.C., Delfour, J., Vialette, Y., 1976. Geochronological measurements (Rb/Sr; K/Ar) on rocks of the Arabian Shield, Kingdom of Saudi Arabia. Saudi Arabia, Dir. Gen. Miner. Resour. Tech. 76, 1–152.

Bea, F., 1996. Controls on the trace element chemistry of crustal melts. The origin of granites and related rocks. Third Hutton Symposium, Maryland, August 26–September 2, 1995, pp. 19–20. Abstracts.

Bentor, Y.K., 1985. The crustal evolution of the Arabo-Nubian Massif with special reference to the Sinai Peninsula. Precambrian Res. 28, 1–74.

Beyth, M., Stern, R.J., Altherr, R., Kröner, A., 1994. The Late Precambrian Timna igneous complex, Southern Israel — evidence for comagmatic-type sanukitoid monzodiorite and alkali granite magma. Lithos 31, 103–124.

Bielski, M., 1982. Stages in the evolution of the Arabo-Nubian massif in Sinai. Ph.D. thesis, Hebrew Univ., Jerusalem (in Hebrew; English Abstract, Tables, Figures).

Bonin, B., 2004. Do coeval mafic and felsic magmas in post-collisional to within-plate regimes necessarily imply two contrasting, mantle and crustal, sources? A review. Lithos 78, 1–24.

Bons, P.D., Arnold, J., Elburg, M.A., Kalda, J., Soesoo, A., van Milligen, B.P., 2004. Melt extraction and accumulation from partially molten rocks. Lithos 78, 25–42.

Brown, W.L., Parsons, I., 1989. Alkali feldspars: ordering rates, phase transformations and behavior diagrams for igneous rocks. Mineral. Mag. 53, 25–42.

Brown, M., Solar, G.S., 1999. The mechanism of ascent and emplacement of granite magma during transpression: a syntectonic granite paradigm. Tectonophysics 312, 1–33.

Chiba, H., Chacko, T., Clayton, R.N., Goldsmith, J.R., 1989. Oxygen isotope fractionations involving diopside, forsterite, magnetite and calcite: application to geothermometry. Geochim. Cosmochim. Acta 53, 2895–2995.

Clayton, R.N., Goldsmith, J.R., Mayeda, T.K., 1989. Oxygen isotope fractionation in quartz, albite, anorthite and calcite. Geochim. Cosmochim. Acta 53, 725–733.

Clemens, J.D., Holloway, J.R., White, A.J.R., 1986. Origin of an A-type granite: experimental constraints. Am. Mineral. 71, 317–324.

Collins, W.J., Beams, S.D., White, A.J.R., Chappell, B.W., 1982. Nature and origin of A-type granites with particular reference to southeastern Australia. Contrib. Mineral. Petrol. 80, 189–200.

Cox, K.G., Bell, J.D., Pankhurst, R.J., 1980. The Interpretation of Igneous Rocks. George Allen & Unwin, London.

Criss, R.E., Taylor, H.P., 1983. An $^{18}O/^{16}O$ and D/H study of Tertiary hydrothermal systems in the southern half of the Idaho batholith. Geol. Soc. Amer. Bull. 94, 640–663.

Criss, R.E., Taylor, H.P., 1986. Meteoric–hydrothermal systems. In: Valley, J.W., Taylor, H.P., O'Neil, J.R. (Eds.), Stable Isotopes in High Temperature Geological. Processes Reviews in Mineralogy, vol. 16. Mineral. Soc. America, Washington, DC, pp. 373–424.

De Paolo, D.J., 1981. Trace element and isotopic effects of combined wall-rock assimilation and fractional crystallization. Earth Planet. Sci. Lett. 53, 189–202.

De Paolo, D.J., Linn, A.M., Schubert, G., 1991. The continental crust age distribution methods to determining mantle separation ages from Sm–Nd isotopic data and application to the southwestern United States. J. Geophys. Res. 96, 2071–2088.

Dingwell, D.B., 1988. The structures and properties of fluorine-rich magmas: a review of experimental studies. In: Taylor, R.P., Strong, D.F. (Eds.), Recent Advances in the Study of Granite-Related Mineral Deposits. Canadian Inst. Mineralogy and Metallogenesis, Montreal, Quebec, pp. 1–12.

Eby, G.N., 1990. The A-type granitoids: a review of their occurrence and chemical characteristics and speculations on their petrogenesis. Lithos 26, 115–134.

Eby, G.N., 1992. Chemical subdivision of the A-type granitoids: petrogenetic and tectonic implications. Geology 20, 641–644.

Eyal, M., Hezkiyahu, T., 1980. Katharina pluton — the outlines of a petrological framework. Isr. J. Earth-Sci. 29, 41–52.

Eyal, M., Shimshilashvili, E., 1988. A comparative album for quantitative study of perthite texture. Isr. J. Earth-Sci. 37, 171–180.

Gass, I.G., 1982. Upper Proterozoic (Pan-African) calc-alkaline magmatism in north-eastern Africa and Arabia. In: Thorpe, R.S. (Ed.), Andesites and Related Rocks. Wiley, Chichester, UK, pp. 595–609.

Genna, A., Nehlig, P., Le Goff, E., Guerrot, C., Shanti, M., 2002. Proterozoic tectonism of the Arabian Shield. Precambrian Res. 117, 21–40.

Goor, A., 1982. Katharina volcanics — an internal ring complex of the High Mountain, southern Sinai. M.S. thesis, Ben-Gurion University of the Negev, Beer-Sheva, Israel (in Hebrew, English Abstract).

Holtz, F., Johannes, W., Tamic, N., Behrens, H., 2001. Maximum and minimum water contents of granite melts generated in the crust: a reevaluation and implications. Lithos 56, 1–14.

Irber, W., 1999. The lanthanide tetrad effect and its correlation with K/Rb, Eu/Eu*, Sr/Eu, Y/Ho, and Zr/Hf of evolving peraluminous granite suites. Geochim. Cosmochim. Acta 63, 489–508.

Jahn, B.-M., 2004. The Central Asian Orogenic Belt and growth of the continental crust in the Phanerozoic. Geol. Soc. Spec. Publ. 226, 73–100.

Jahn, B.-M., Cornichet, J., Cong, B.-L., Yui, T.-F., 1996. Ultrahigh-ε_{Nd} eclogites from an ultrahigh-pressure metamorphic terrane of China. Chem. Geol. 127, 61–79.

Jahn, B.-M., Wu, F.Y., Chen, B., 2000. Granitoids of the Central Asian Orogenic Belt and continental growth in the Phanerozoic. Trans. R. Soc. Edinb. Earth Sci. 91, 181–193.

Jahn, B.-M., Wu, F.Y., Capdevila, R., Martineau, F., Zhao, Z., Wang, Y., 2001. Highly evolved juvenile granites with tetrad REE patterns: the Woduhe and Baerzhe granite from the Great Xing'an Mountains in NE China. Lithos 59, 171–198.

Jahn, B.-M., Capdevila, R., Liu, D., Vernov, A., Badarch, G., 2004. Sources of Phanerozoic granitoids in the transect Bayanhongor-Ulan Baator, Mongolia: geochemical and Nd isotopic evidence, and implications of Phanerozoic crustal growth. J. Asian Earth Sci. 23, 629–653.

James, R.S., Hamiltin, D.L., 1969. Phase relations in the system $NaAlSi_3O_8$–$KAlSi_3O_8$–$CaAl_2Si_2O_8$–SiO_2 at 1 kilobar water vapour pressure. Contrib. Mineral. Petrol. 21, 111–141.

Jarrar, G., Baumann, A., Wachendorf, H., 1983. Age determinations in the Precambrian rocks of the Wadi Araba area, southwest Jordan. Earth Planet. Sci. Lett. 63, 292–304.

Johannes, W., Holtz, F., 1996. Petrogenesis and Experimental Petrology of Granitic Rocks. Springer-Verlag, Berlin.

King, E.M., Valley, J.W., Tucker Barrie, C., 1997. Hydrothermal alteration of oxygen isotope ratios in quartz phenocrysts, Kidd Creek Mine, Ontario: magmatic values are preserved in zircon. Geology 25, 1079–1082.

Kovalenko, N.I., 1978. The reaction between granite and aqueous hydrofluoric acid in relation to the origin of fluorine-bearing granites. Geochem. Int. 14, 108–118.

Kröner, A., Greiling, R., Reischmann, T., Hussein, I.M., Stern, R.J., Durr, S., Krugger, J., Zimmer, M., 1987. Pan-African crustal evolution in the Nubian segment of north-eastern Africa. In: Kröner, A. (Ed.), Proterozoic Lithospheric Evolution Am. Geophys. Union Geodynanic Series, vol. 15, pp. 235–257.

Lee, M.R., Waldron, K.A., Parsons, I., 1995. Exsolution and alteration microtextures in alkali feldspar phenocrysts from the Shap granite. Mineral. Mag. 59, 63–78.

Le Maitre, R.W. (Ed.), 1989. A Classification of Igneous Rocks and Glossary of Terms. Blackwell, Oxford.

Leitch, A.M., Weinberg, R.F., 2002. Modelling granite migration by mesoscale pervasive flow. Earth Planet. Sci. Lett. 200, 131–146.

Liégeous, J.-P., Black, R., 1987. Alkaline magmatism subsequent to collision in the Pan-African belt of the Adrar des Iforas. In: Fitton, J.G., Upton, B.G.J. (Eds.), Alkaline Igneous RocksGeol. Soc. Spec. Publ., vol. 30, pp. 381–401.

Litvinovsky, B.A., Steel, I.M., Wickham, S.M., 2000. Silicic magma formation in overthickened crust: melting of charnockite and leucogranite at 15, 20 and 25 kbar. J. Petrol. 41, 717–737.

Litvinovsky, B.A., Jahn, B.-M., Zanvilevich, A.N., Saunders, A., Poulain, S., 2002. Petrogenesis of syenite–granite suites from the Bryansky Complex (Transbaikalia, Russia): implications for the origin of A-type granitoid magmas. Chem. Geol. 189, 105–133.

Loiselle, M.C., Wones, D.R., 1979. Characteristics and origin of anorogenic granites. Geol. Soc. Am. Abstr. Progr. 11, 468.

London, D., 1986. Magmatic–hydrothermal transition in the Tanco rare-element pegmatite: evidence from fluid inclusions and phase-equilibrium experiments. Am. Mineral. 71, 376–395.

London, D., 1987. Internal differentiation of rare-element pegmatite: effect of boron, phosphorus and fluorine. Geochim. Cosmochim. Acta 51, 403–420.

Ludwig, K.R., 2003. ISOPLOT/Ex 3.00. A geochronological toolkit for microsoft excel. Berkeley Geochronology Center Sp. Publ., vol. 4. 70 pp.

Maniar, P.D., Piccoli, P.M., 1989. Tectonic discrimination of granitoids. Geol. Soc. Amer. Bull. 101, 635–643.

Meert, J.G., 2003. A synopsis of events related to the assembly of eastern Gondwana. Tectonophysics 362, 1–40.

Moghazi, A.M., 1999. Magma source and evolution of Late Neoproterozoic granitoids in the Gabal El–Urf area, Eastern Desert, Egypt: geochemical and Sr–Nd isotopic constraints. Geol. Mag. 136, 285–300.

Moghazi, A.M., Andersen, T., Oweiss, G.A., El Bouseily, A.M., 1998. Geochemical and Sr–Nd–Pb isotopic data bearing on the origin of Pan-African granitoids in the Kid area, southeast Sinai, Egypt. J. Geol. Soc. (Lond.) 155, 697–710.

Moghazi, A.M., Mohamed, F.H., Kanisawa, S., 1999. Geochemical and petrological evidence of calc-alkaline and A-type magmatism in the Homrit Waggat and El-Yatima areas of eastern Egypt. J. Asian Earth Sci. 29, 535–549.

Nash, W.P., Crecraft, H.R., 1985. Partition coefficients for trace elements in silicic magmas. Geochim. Cosmochim. Acta 49, 2309–2322.

O'Neil, J.R., Taylor, H.P., 1967. The oxygen isotope and cation exchange chemistry of feldspars. Am. Mineral. 52, 1414–1437.

O'Neil, J.R., Clayton, R.N., Mayeda, T.K., 1969. Oxygen isotope fractionation in divalent metal carbonates. J. Chem. Phys. 51, 5547–5558.

Orville, P.M., 1963. Alkali ion exchange between vapor and feldspar phases. Am. J. Sci. 261, 201–237.

Parsons, I., 1978. Feldspars and fluids in cooling plutons. Mineral. Mag. 42, 1–17.

Patiño Douce, A.E., 1997. Generation of metaluminous A-type granites by low-pressure melting of calc-alkaline granitoids. Geology 25, 743–746.

Pearce, J.A., Harris, N.B.W., Tindle, A.G., 1984. Trace element distribution diagrams for the tectonic interpretation of granitic rocks. J. Petrol. 25, 956–983.

Ponader, C.W., Brown, G.E., 1989. Rare earth elements in silicate glass/melt system. II. Interaction of La, Gd and Yb with halogens. Geochim. Cosmochim. Acta 53, 2905–2914.

Reyf, F.G., Bazheev, Y.D., 1985. Determination principles of ore bearing (Mo–W–Sn) granites and their thermobarogeochemical features. Geol. zb.— Geol. Carpatica 36, 375–384.

Rogers, J.J.W., Satterfield, M.E., 1994. Fluids in anorogenic granites: a preliminary assessment. Mineral. Petrol. 50, 157–171.

Spicuzza, M.J., Valley, J.W., Kohn, M.J., Girard, J.P., Fouillac, A.M., 1998a. The rapid heating, defocused beam technique: a CO_2-laser-based method for highly precise and accurate determination of $\delta^{18}O$ values of quartz. Chem. Geol. 144, 195–203.

Spicuzza, M.J., Valley, J.W., McConnell, V.S., 1998b. Oxygen isotope analysis of whole rock via laser fluorination: an air-lock approach. Geol. Soc. Am. Abstr. Progr. 30, 80.

Stein, M., Goldstein, S.L., 1996. From plume head to continental lithosphere in the Arabian–Nubian shield. Nature 382, 773–778.

Stern, R.J., 1994. Neoproterozoic (900–550 Ma) arc assembly and continental collision in the East African orogen: implications for the consolidation of Gondwanaland. Annu. Rev. Earth Planet. Sci. 22, 319–351.

Stern, R.J., Hedge, C.E., 1985. Geochronologic and isotopic constraints on Late Precambrian crustal evolution in the Eastern Desert of Egypt. Am. J. Sci. 285, 97–127.

Stern, R.J., Kröner, A., 1993. Late Precambrian crustal evolution in NE Sudan, isotopic and geochronologic constraints. J. Geol. 101, 555–574.

Stern, R.J., Gottfried, D., Hedge, C.E., 1984. Late Precambrian rifting and crustal evolution in the Northeastern Desert of Egypt. Geology 12, 168–172.

Stix, J., Gorton, M.P., 1990. Variations in trace element partition coefficients in sanidine in the Cerro Toledo rhyolite, Jemez Mountains, New Mexico: effects of composition, temperature, and volatiles. Geochim. Cosmochim. Acta 54, 2697–2708.

Sun, S., McDonough, W.F., 1989. Chemical and isotopic systematics of oceanic basalts, implications for mantle compositions and processes. In: Saunders, A.D., Norry, M.J. (Eds.), Magmatism in the Ocean BasinsGeol. Soc. Spec. Publ., vol. 42, pp. 313–345.

Taylor, H.P., 1968. The oxygen isotope geochemistry of igneous rocks. Contrib. Mineral. Petrol. 19, 1–71.

Taylor, H.P., 1977. Water/rock interaction and the origin of H_2O in granitic batholiths. J. Geol. Soc. (Lond.) 133, 509–558.

Taylor, H.P., 1978. Oxygen and hydrogen isotope studies of plutonic granitic rocks. Earth Planet. Sci. Lett. 38, 177–210.

Taylor, H.P., Sheppard, S.M.F., 1986. Igneous rock: I. Processes of isotopic fractionation and isotope systematics. In: Valley, J.W., Taylor, H.P., O'Neil, J.R. (Eds.), Stable Isotopes in High Temperature Geological Processes. Reviews in Mineralogy, vol. 16. Mineral. Soc. America, Washington, DC, pp. 227–271.

Turner, S.P., Foden, J.D., Morrison, R.S., 1992. Derivation of some A-type magmas by fractionation of basaltic magma: an example from the Padthway Ridge, South Australia. Lithos 28, 151–179.

Tuttle, O.F., Bowen, N.L., 1958. Origin of granite in light of experimental studies in the system $NaAlSi_3O_8$–$KAlSi_3O_8$–SiO_2–H_2O. Geol. Soc. Am., Mem. 74 (153 pp.).

Valley, J.W., 2001. Stable isotope thermometry at high temperatures. In: Valley, J.W., Cole, D.R. (Eds.), Stable Isotope Geochemistry. Reviews in Mineralogy and Geochemistry, vol. 43. Mineral. Soc. America, Washington, DC, pp. 365–414.

Valley, J.W., 2003. Oxygen isotopes in zircon. In: Hanchar, J.M., Hoskin, W.O. (Eds.), Zircon. Reviews in Mineralogy and Geochemistry, vol. 53. Mineral. Soc. America, Washington, DC, pp. 343–385.

Valley, J.W., Chiarenzelli, J.R., McLelland, J.M., 1994. Oxygen isotope geochemistry of zircon. Earth Planet. Sci. Lett. 126, 187–206.

Valley, J.W., Kitchen, N., Kohn, M.J., Niendorf, C.R., Spicuzza, M.J., 1995. UWG-2, a garnet standard for oxygen isotope ratios: strategies for high precision and accuracy with laser heating. Geochim. Cosmochim. Acta 59, 5223–5231.

Vallley, J.W., Bindeman, I.N., Peck, W.H., 2003. Empirical calibration of oxygen isotope fractionation in zircon. Geochim. Cosmochim. Acta 67, 3257–3266.

Valley, J.W., Lackey, J.S., Cavosie, A.J., Clechenko, C.C., Spicuzza, M.J., Basei, M.A.S., Bindeman, I.N., Ferreira, V.P., Sial, A.N., King, E.M., Peck, W.H., Sinha, A.K., Wei, C.S., 2005. 4.4 billion years of crustal maturation: oxygen isotope ratios of magmatic zircon. Contrib. Mineral. Petrol. 150, 561–580.

Van der Molen, I., Peterson, M.S., 1979. Experimental deformation of partially-melt granite. Contrib. Mineral. Petrol. 70, 299–318.

Vielzeuf, J.D., Clemens, C.P., Moinet, E., 1990. Granites, granulites, and crustal differentiation. In: Vielzeuf, J.D., Vidal, Ph. (Eds.), Granulites and Crustal Evolution Series C: Mathematical and Physical Sciences. Kluwer Acad. Publishers, pp. 59–85.

Vigneresse, J.L., Barbey, P., Cuney, M., 1996. Rheological transitions during partial melting and crystallization with application to felsic magma segregation and transfer. J. Petrol. 37, 1579–1600.

Walker, F.D.L., Lee, M.R., Parsons, I., 1995. Micropores and micropermeable texture in alkali feldspar: geochemical and geophysical implications. Mineral. Mag. 59, 505–534.

Weinberg, R.F., 1999. Mesoscale pervasive felsic magma migration: alternatives to dyking. Lithos 46, 393–410.

Whalen, J.B., Currie, K.L., Chappel, B.W., 1987. A-type granites: geochemical characteristics, discrimination and petrogenesis. Contrib. Mineral. Petrol. 95, 407–419.

Whalen, J.B., Jenner, J.A., Longstaffe, F.J., Robert, F., Gariepy, C., 1996. Geochemical and isotopic (O, Nd, Pb and Sr) constraints on A-type granite petrogenesis based on the Topsails igneous suite, Newfoundland Appalachians. J. Petrol. 37, 1463–1489.

White, A.J.R., Chappell, B.W., 1983. Granitoid types and their distribution in the Lachlan fold belt, southeastern Australia. Geol. Soc. Amer. Bull. 159, 21–34.

Wickham, S.M., Litvinovsky, B.A., Zanvilevich, A.N., Bindeman, I.N., 1995. Geochemical evolution of Phanerozoic magmatism in Transbaikalia, East Asia: a key constraint of the origin of K-rich silicic magmas and the process of cratonization. J. Geophys. Res. 100/B8, 15641–15654.

Worden, R.H., Walker, F.D.L., Brown, W.L., 1990. Development of microporosity, diffusion channels and deuteric coarsening in perthitic alkali feldspars. Contrib. Mineral. Petrol. 104, 507–515.

Wu, F.-Y., Sun, D.-Y., Li, H.-M., Jahn, B.-M., Wilde, S.A., 2002. A-type granites in Northeastern China: age and geochemical constraints on their petrogenesis. Chem. Geol. 187, 143–173.

Wu, F.-Y., Sun, D.-Y., Jahn, B.-M., Wilde, S.A., 2004. A Jurassic garnet-bearing granitic pluton from NF China showing tetrad REE patterns. J. Asian Earth Sci. 23, 731–744.

Yoder, H.S., Steward, D.B., Smith, J.R., 1957. Ternary feldspars. Year Book - Carnegie Inst. Washington 55, 206–214.

Zanvilevich, A.N., Litvinovsky, B.A., Wickham, S.M., Bea, F., 1995. Genesis of alkaline and peralkaline syenite–granite series: the Kharitonovo pluton (Transbaikalia, Russia). J. Geol. 103, 127–145.